# A RAPID MALARIA DIAGNOSTIC METHOD BASED ON AUTOMATIC DETECTION AND CLASSIFICATION OF *PLASMODIUM* PARASITES IN STAINED THIN BLOOD SMEAR IMAGES

M.Sc. Thesis

By

Daniel Maitethia Memeu

B.Sc. (Hons,)

Department of Physics, University of Nairobi.

***A thesis submitted in partial fulfillment of the degree of Master of Science in Physics at the University of Nairobi, March, 2014.***

# Declarations

**This work is my own and has not been submitted in any other university**

……..

Daniel Maitethia Memeu,

Department of Physics,

University of Nairobi.

**This thesis has been submitted for examination with our approval as university Supervisors:**

Dr. Kenneth Amiga Kaduki.

Department of Physics, University of Nairobi.

Signature……. Date…….

Mr. A.C.K. Mjomba

Department of Physics, University of Nairobi.

Signature……. Date…….

# Abstract

Malaria is the leading cause of morbidity and mortality in tropical and subtropical countries. Conventional microscopy used in diagnosis of the disease has occasionally proved inefficient since it is time consuming and results are difficult to reproduce. Alternative diagnosis techniques which yield superior results are quite expensive and hence inaccessible to developing countries where the disease is endemic.

In this work, an accurate, rapid and affordable model of malaria diagnosis using stained thin blood smear images was developed. The method makes use of the morphological, colour and texture features of*Plasmodium* parasites and erythrocytes. Images of infected and non-infected erythrocytes were acquired, pre-processed, relevant features extracted from them and eventually diagnosis was made based on the features extracted from the images. Diagnosis entailed detection of *Plasmodium* parasites, differentiation of different *Plasmodium* parasite stages and species, as well as parasitemia estimation.

Image pre-processing entailed reducing the size of the acquired images to speed up processing and median filtering to remove salt and pepper noise. Neural network classifiers were then trained and used to detect and determine the life stages and species of *Plasmodium* parasites. Template matching technique was used to approximate the number of erythrocytes in the images and hence estimate the degree of infection (parasitemia).

Classification accuracy of 95.0%, 92.7%, 92.0%, and 79.7% for detection of infected erythrocytes, stages determination, species identification, and parasitemia estimation respectively was achieved with respect to results obtained by expert microscopists. The study revealed that artificial neural network (ANN) classifiers trained with colour, morphological, and texture features of infected stained thin blood smear images are suitable for detection and classification of *Plasmodium* parasites into their respective stages and species. It was further shown that ANN classifiers can be trained to perform image segmentation.

# Acknowledgements

This work has been a success as a result of the efforts of many people whom I cannot mention them all by name. However, my gratitude first goes to my supervisors; Mr. A.C .K. Mjomba and Dr. K. A. Kaduki for their constant supervision and guidance.

I also want to acknowledge the University of Nairobi NindhiSmarakScholarship fund, for the financial assistance they accorded me in the course of my studies, without which this work would not be possible. On the same breath I acknowledge the technical staff of the University of Nairobi, particularly Mr. Dickson Omucheni for his invaluable assistance. I am equally grateful to International Science Program for their assistance that enabled me to acquire a computer which I was using to carry out my research.

Last but not least my heartfelt appreciation goes to my family and friends for their love and support.

# List of Abbreviations and Acronyms

**ANN** -Artificial Neural Networks

**AUC** - Area Under Curve

**CDC** -Centre for Disease Control

**CMY** -Cyan Magenta Yellow

**CMYK** -Cyan Magenta Yellow Black

**HCA** -Hierarchical Cluster Analysis

**HSI** -Hue Saturation and Intensity

**HSV** -Hue Saturation Value

**IR** -Infra Red

**KEMRI** -Kenya Medical Research Institute

**LEDs** -Light Emitting Diodes

**PCR** -Polymerase Chain Reaction

**PCA** -Principal of Components Analysis

**RBCs** -Red Blood Cells

**RDT** -Rapid Diagnostic Tests

**RGB** -Red Green Blue

**ROC** -Receiver Operating Characteristic

**SE** -Structuring element

**THG** -Third Harmonic Generation

**UV** -Ultra Violet

**WBCs** -White Blood Cells

# List of Figures

# List of Tables

# Table of Contents

# CHAPTER 1: INTRODUCTION

Malaria is a common but serious protozoan disease caused by peripheral blood, spleen or liver parasites of the genus *Plasmodium*. There are four species of *Plasmodium* parasites that cause malaria in humans. These are *Plasmodium falciparum, Plasmodiumovale, Plasmodiumvivax*and*Plasmodium malariae*. These species of *Plasmodium* attack red blood cells and undergo various life stages namely, early trophozoites, mature trophozoites, gametocytes and schizoites.

It is estimated that approximately 781,000 people of the 225 million people infected worldwide by the disease succumb to this menace annually [1]. Majority of these deaths are children from sub-Saharan Africa [2]. In Kenya malaria accounts for 30 – 50% of all outpatient attendance and 20% of all admissions in health facilitates. It is also estimated that 20% of all deaths of children under five years is due to malaria [3].The disease causes a heavy economic burden to those affected in terms of the costs incurred to treat the disease and absenteeism from work and school.

Several methods exist for malaria diagnosis. These methods can be classified into two, based on their cost and performance. These are the high cost methods and low cost methods. Polymerase Chain Reaction (PCR)-based techniques that detect specific nucleic acid sequences [4] and Third Harmonic Generation (THG) imaging of *Hemozoin*using infrared ultrafast pulsed laser excitation, belong to the class of high cost methods.*Plasmodium* parasites in unstained thin blood smears have been detected using THG imaging microscope [5]. These techniques can yield high sensitivity and specificity to malaria diagnosis;however, they are rarely used in developing countries where the disease is endemic because of their high cost, specialized infrastructure needs and handling difficulties.Rapid Diagnostic Test (RDT) which detects specific antigens derived from malaria parasites in lysed blood [6] and conventional microscopy [7, 8] belong to the low cost class.While RDT are relatively fast in malaria diagnosis and can be administered by less skilled personnel, their results can be unreliable [8]. Besides, the commercially available RDT kits are specific to single species of *Plasmodium* parasites and in cases where a patient is infected with multiple species of *Plasmodia*, different kits should be used, an approach which makes the cost of diagnosis

to go up.The key to effective management of malaria lies in prompt and accurate diagnosis of the disease.

Conventional microscopy is the gold standard for malaria diagnosis. In this method, peripheral blood from a patient is drawn and a smear made on a glass slide. This smear is then stained with a chemical called Giemsa. Staining helps to differentiate between *Plasmodium* parasites and red blood cells.The most serious limitations of this technique are that it is time consuming, the results obtained are difficult to reproduce and the personnel that conduct the test should be skilled. The last challenge can be can be quite serious in areas where the disease is endemic or has limited number of skilled human capacity.

From the above discussion of malaria diagnosis methods, it can be in that the more sophisticated the technique becomes, the more reliable the result of the diagnosis. However, this advantage is achieved at the expense of increased cost and reduced accessibility of diagnostic facilities. The low cost of less sophisticated diagnostic techniques have higher risks associated with poor clinical outcomes.Low cost malaria diagnosis techniques can be improved by incorporating some processing component in their outputs. As a result we can devise a new framework of classifying malaria diagnosis techniques based on the complexity involved in detection and processing. This scheme would therefore yield four classes of diagnosis techniques. These classes are summarized in the Figure 1.1.

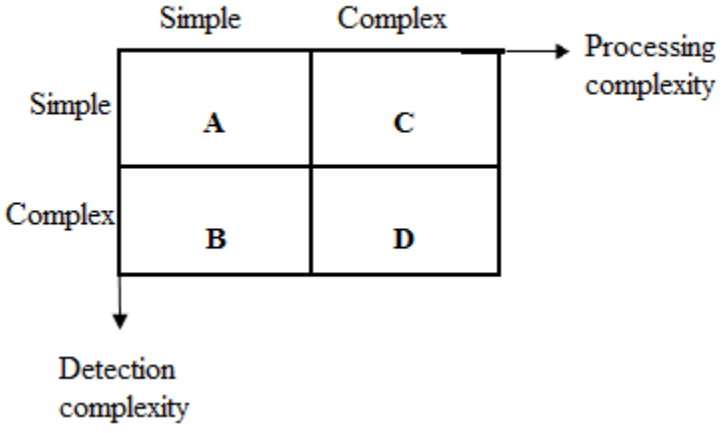


**Figure 1.1: Malaria classification schemes based on detection and processing as coordinates**

FromFigure 1.1, the ideal diagnosis technique would be that from class A, however, no such technique has been developed with acceptable accuracy. Class D is the least desirable category because it call for expensive detection and processing schemes. This would translate to high cost of installation, operation and high skilled personnel requirement. This leaves us with class B and C as our methods of choice. Most conventional diagnosis techniques would fall in class C, where effort is placed in detection and very little processing if any is carried out. As a result of the sophisticated apparatus required, the process ends up being expensive and sometimes out of reach. Class B calls for simple detection scheme and complex processing algorithms. Simple detection and complex processing is feasible since the semiconductor industry has made tremendous improvements in fabrication of low cost and high speed computer processors.

Because of these desirable features, a class B scheme of malaria diagnosis was explored in this work. An automatic method of detecting and classifying *Plasmodium* parasites into their respective stages and species as well as determining the degree of infection was investigated. Image processing and machine learning techniques were utilized to solve this problem. The ultimate goal of the study was to develop a fast, accurate and affordable technique for malaria diagnosis using images of stained thin blood smears. Stained blood smear images were acquired and preprocessed. Relevant features were then extracted and classified using neural network classifiers. The system gave status on the degree of malaria infection, life stage and species of the *Plasmodium* parasite. High rates of sensitivity and specificity in parasitemia detection were recorded. The block diagram for the developed system is depicted in the Figure 1.2.

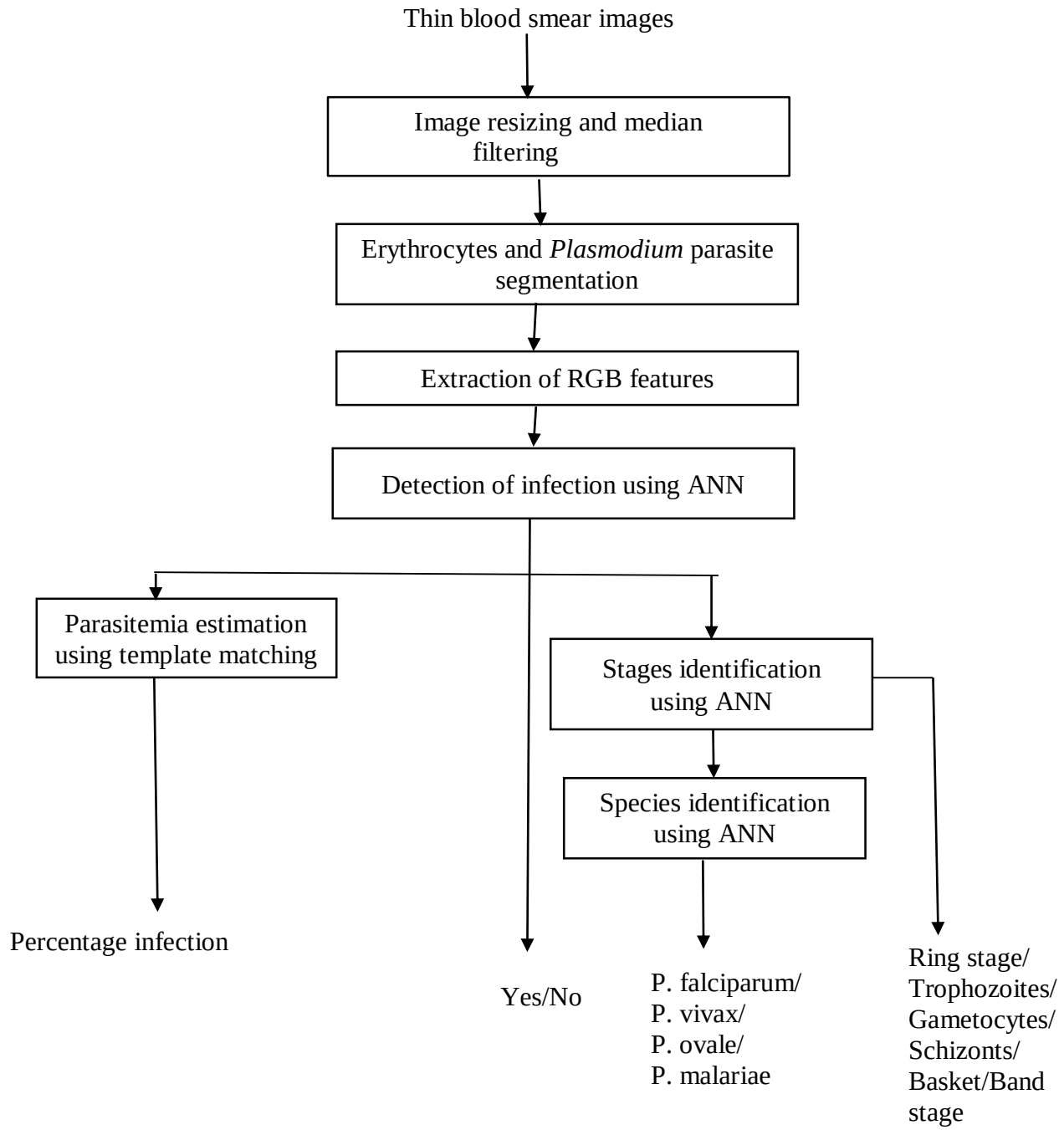


**Figure 1.2: Block diagram of the automated malaria diagnosis technique**

This thesis is written in six chapters: Chapter 1 introduces various malaria diagnosis techniques and briefly summarizes their pros and cons. Chapter 2 discusses related work that has been carried out by other researchers: It spells out the objectives and significance of the study. The shortcomings of the preceding work and what the current work seeks to solve are highlighted. Chapter 3 lays down the theoretical framework of the techniques used in this work. A discussion of image processing and machine learning techniques is presented here. These techniques are thereafter applied in Chapter 4 which gives an account of the methodology.This chapter is divided into three main sections namely; the process model which illustrates an overview of the scheme used to develop a malaria diagnosis system using images of thin blood smear, diagnosis system methodologyand algorithms for classification and parasitemia estimation. In the diagnosis system methodology, different techniques for detection of *Plasmodium* parasite, stages and species identification and parasitemia estimation are explored and their test results presented. A decision is thereafter made on the best techniques to use in developing a malaria diagnosis system. Based on this decision, algorithms are developed for detection, stages and species classification of *Plasmodium* parasite as well as parasitemia estimation. Chapter 5 presents the results obtained. The resultsare evaluated in four main sub-tasksnamely, detection of infected erythrocytes, determination of parasite species and stages, and parasitemia estimation. The main findings and weaknesses of the study are discussed and future research work is suggested in Chapter 6.

# CHAPTER 2: LITERATURE REVIEW

## 2.1 Overview of Malaria Diagnosis Approaches

A number of confirmatory tests for *Plasmodium* parasites exist. These techniques can be categorized into two classes depending on their level of detection complexity and cost of installation. These are the low cost, low technology techniques and the high cost, high technology techniques. The low level techniques include the conventional microscopy and Rapid Diagnostic Tests (RDTs) while the high level techniques include the Polymerase Chain Reaction (PCR) and Third Harmonic Generation (THG) imaging test. A briefdescription of these techniques is given below.

### 2.1.1Conventional Microscopy

This is currently the gold standard in malaria diagnosis since it is relatively cheap and allows quantification of parasitemia and determination of *Plasmodium* parasite life stages and species. However, the technique suffers from some limitations, with the most serious being that the method is time consuming, especially when parasitemia is low. This is because many microscopic fields of view have to be examined before a decision of the diagnosis is made. Besides, in the case of mixed infections the microscopist has to examine the slides carefully in order to differentiate between different species of *Plasmodium* present. Also he/she has to take account of the fact that some parasite stages remain in the blood for a while after treatment of the disease [9]. The sensitivity of the technique is also affected by malaria parasite density in blood [4, 10]. The results are difficult to reproduce and the accuracy of the method depends on the skills and experience of the microscopist [11 - 13].

### 2.1.2 Rapid Diagnostic Tests (RDTs)

These are alternative methods of malaria diagnosis recommended by W.H.O. for use in areas where microscopy is not available [8]. The methods detect antigens derived from malaria parasites. They are faster than the conventional microscopy with a single diagnosis taking an average time

of 30 minutes [14]. Besides, the techniques can be administered by a non-skilled technician. Some of these methods include Parasight-F [6], ICT Malaria pf/pv [15], and optiMAL [16]. The methods suffer from limitations including: low sensitivity over microscopy [17], and prevalence of false positives particularly after treatment [18].

### 2.1.3 Polymerase Chain Reaction (PCR)

This is a sophisticated technique which requires advanced infrastructure. PCR is used to amplify a single or a few copies of DNA sequence to several orders of magnitude. The technique is used in medical and research laboratories for several applications including diagnosis of malaria [12 – 14, 20 - 22] and requires several components and reagents [23]. When used for malaria diagnosis, PCR has several advantages including, high sensitivity even in low parasite load [12, 23 - 25], and ability to distinguish different species of *Plasmodium* parasites. This technique, however, suffers from some limitations such as: high cost of installing its infrastructure, inability to quantify parasitemia and long diagnosis duration with a single case taking up to 8 hours [14].

### 2.1.4 Third Harmonic Generation (THG) Imaging

Third Harmonic Generation (THG) imaging with femtosecond laser excitation can be used to detect malaria pigment (*Hemozoin*) [5, 26]. However, just like PCR, the technique has not so far been adopted in malaria endemic zones due to its high cost of installation and its demand for highly skilled manpower.

### 2.1.5 Related Work

A number of studies on the possibility of automating conventional microscopy have been done in the past. In this section a number of these studies are reviewed.

Zoueu*et al.* (2008), [27] proposed a method of diagnosing malaria without labelling the parasites using a light microscope with LEDs emitting in the range of UV to IR replacing the classic white light. The microscope was fitted with a digital camera to capture images formed at the eye piece.

It was reported that parasite images having the best contrast were recorded for blue light. This study, however, failed to address the effects of chromatic aberration which are common in multispectral imaging using classical optics. Chromatic aberration causes images of specimen in a light microscope to be formed in different focal points for different wavelengths of light used to illuminate the specimen. This would therefore pose a challenge in automating the detection and classification of *Plasmodium* parasites because adjustment of focal point would be required for every wavelength used for illumination. The technique was also dependent of a human operator for switching between LEDs and making the diagnosis.

Brydegaard*et. al*.(2011), [28], proposed an improved version of multispectral microscope based on light emitting diodes (LEDs). The LEDS emitted lights in 13 spectral bands ranging from ultra-violet (UV) to near infra-red (IR). The dispersive optical components of the instrument were made of quartz to reduce achromatic aberration and lens fluorescence in illumination profiles towards the ultraviolent region. The device was also fitted with an imager for capturing images in the 13 spectral range of the LEDs. The instrument was interfaced to a computer and switching of LEDs and image capturing was done using LAB-VIEW software. It was reported that the instrument could detect *Plasmodium* parasites in non-stained thin blood smear images. However, species and stages differentiation of *Plasmodium* parasites was not addressed.

Omucheni*et. al.* (2012), [29] developed a technique of detecting *Plasmodia* infected erythrocytes by imaging unstained thin blood smear blood samples using a multispectral imaging microscope developed by Bryegaard [28]. Multivariate chemometric techniques such as Principal of Components Analysis (PCA), Hierarchical Cluster Analysis (HCA) and Artificial Neural Network (ANN) were used to process the multispectral images obtained in order to discriminate infected erythrocytes from the non-infected. *Plasmodium* parasites stages and species identification was not addressed.

Ross *et. al.*(2006), [30] proposed a technique for automating malaria diagnosis using optical microscopy. A light microscope fitted with a digital camera was used to capture images of Giemsa stained blood slides. After images were captured they were loaded to a Personal Computer (PC) for processing.Image processing techniques and neural network classifiers were used. Infected

erythrocytes were positively identified with a sensitivity of 81% while the sensitivity for species determination was 73%. The study did not address the quantification of parasitemia and determination of parasite species. Morphological image processing techniques used for erythrocyte segmentation could not produce satisfactory results as erythrocytes were heavily clustered [31]. The sizes of erythrocytes were determined using granulometry with circular structuring element (SE). The assumption was erythrocyte shapes are circular. This is not always the case. Sometimes erythrocytes shapes are deformed especially if they are infected with diseases such as sickle cell or if they appear in clusters [31].

Diaz*et. al.*(2009), [32] developed a technique for detection, quantification of parasitemia and parasite life stages. Pixel colour features were extracted and used to train classifiers for detection and determination of parasite life stages. Clustered erythrocytes were resolved by use of template matching before parasitemia was estimated. The study reported a sensitivity of 94% for detection of infected erythrocytes and 79% for stages identification. The technique was not fully automatic as it called for human intervention during training of the classifier every time diagnosis had to be made. Besides being semi-automatic, the process of erythrocyte identification and stage determination were computationally expensive as features for classification were extracted from every single pixel in the image.

Di Rubert*oet. al.*(2002), [33] proposed a technique of automatically detecting and quantifying malaria parasites infection in blood images of patients. The method employed a modified watershed algorithm to segment erythrocytes. There were two alternatives proposed for classifying parasite stages. One was the use of morphological thinning, where skeletons of parasites images were used to categorize parasitesinto their respective stages of infection. The second option was use of colour histograms similarity. The study did not propose a technique of differentiating species of *Plasmodium* parasites. The efficiency of the segmentation algorithm proposed reduces with the degree of clustering of erythrocytes. Similarly the accuracy of colour histogram similarity for classification of parasites would depend on the imaging parameters and illumination conditions under which the image being probed is taken. The detection accuracy of parasitemia reported was relatively low at 50%.

Anand*et. al.*,(2012)[34]investigated detection of *Plasmodium* infected erythrocytes using a technique called holography. A digital holographic microscope was set up to capture holograms of erythrocytes. A mathematical reconstruction algorithm was then applied to the holograms to recover the object wave. To differentiate between a health cell and an infected cell, a correlation operation was performed using thickness profiles of the reconstructed image with the thickness profile of a known health erythrocyte. Detection probabilities of 84% and 11% as true positive rates and false positive rates were reported. This technique does not involve staining of erythrocyte before detection. However, setting up the digital holographic microscope demands thorough alignment of the optics involved which would require skilled personnel.

In summary, it can be seen that no study has been done so far that comprehensively addresses malaria diagnosis from detection of *Plasmodium* parasites to determination of life stages and species of the parasites as well as parasitemia estimation. Besides, most of the techniques proposed in the previous works provide over simplified methods which are not realistic. For instance some studies have not addressed the distinction of *Plasmodium* parasites from the rest of stained objects (artefacts) in the blood sample [31].

In this work, most of the limitations of the previous works have been addressed. For instance, a novel method of segmenting erythrocytes and *Plasmodium* parasites using artificial neural networks (ANN) has been developed. This technique has solved the problem of distinguishing between the *Plasmodium* parasites and other stained objects (artefacts) in images of thin blood smears. Identification of erythrocytes is performed byANN classifier. The classifier is trained to recognize erythrocytes with varied features. This makes the technique more robust than granulometry which has been used extensively in previous studies in erythrocyte recognition [32, 33]. Segmentation of clustered erythrocytes has been implemented by template matching technique with different possible shapes of erythrocytes used as templates. This has improved the accuracy of determining parasitemia.

## 2.2 Statement of the Problem

Conventional microscopy is the recommended method for malaria diagnosis. However, this method is time consuming, labour intensive and reliability of the results depends on the skills and experience of the microscopist. These limitations can be minimized by automating the process. No previous study has comprehensively solved the problem of malaria diagnosis using images of thin blood smears. The major problems encountered in these studies have been; segmentation of erythrocytes and actual *Plasmodium* parasites, distinguishing between *Plasmodium* parasites and artefacts, differentiating between different species and stages, and parasitemia estimations especially in clustered erythrocytes. In this work, an improvedmethod of malaria diagnosis using images of stained thin blood smears has been developed. A novel technique of segmenting erythrocytes and *Plasmodium* parasites was developed. Species and *Plasmodium* life stages were identified using ANN classifiers using colour, morphological and textural features. The classifier has the ability to distinguish *Plasmodium* parasites from other stained objects in blood smear images.

## 2.3 Objectives

The aim of this research was to develop a system that would offer speedy and accurate malaria diagnosis in human blood media based on the colour and morphological features of *Plasmodium* parasites and infected erythrocytes. The specific objectives were as follows:

1. To develop suitable algorithms for:
   (a) Detecting *Plasmodium* parasites
   (b) Classifying the parasites into their respective species
   (c) Classifying the parasites into their life stages
   (d) Estimating parasitemia
2. To assess the accuracy of the developed algorithms in:
   (a) *Plasmodium* parasite stages differentiation
   (b) *Plasmodium* parasite species differentiation
   (c) Parasitemia estimation

## 2.4 Justification and Significance of the Study

Majority of malaria diagnosis techniques usually require human intervention to aid in interpretation of their results. Attempts to automate conventional microscopy which is the gold standard method of malaria diagnosis has yielded little success as the degree of accuracy for parasitemia estimation and species differentiation reported remains low. This work was aimed at developing a fully automated malaria diagnosis system that would process images of malaria samples and provide all the necessary details with improved accuracy. The developed system can be used for diagnosing other blood vectors by training the ANN classifiers with appropriate features. A reliable, accurate and speedy malaria diagnosis technique will significantly help in management of the malaria menace and reduce the economic burden that the disease causes to many developing nations.

# CHAPTER 3: THEORETICAL BACKGROUND

This chapter presents the theoretical background of an image recognition problem.An image recognition problem undergoes the following sequence of steps:

i. Image acquisition
ii. Image pre-processing
iii. Image segmentation
iv. Feature extraction
v. Individual object recognition
vi. Image understanding

Image acquisition involves formation of an image in an image capturing device such as a camera. Image pre-processing makes the image more suitable for subsequent processing. Image segmentation can be defined as the process of assigning a label to every pixel in an image. The next step is extraction of suitable features from an image by use of appropriate image processing techniques. Based on features extracted, a classification of individual objects present in an image is undertaken using a classifier. The last step in an image recognition process is image understanding or 'making sense' of an ensemble of recognized objects. Here a decision is made of what the image scene is all about based on the recognised objects in the image.

## 3.1 Image Acquisition

### 3.1.1 Image Formation

An image is formed when light from a source is either reflected or transmitted by a scene (object) and then received by an imaging device. An image therefore, has two components namely, the amount of source illumination present on the scene being viewed, and the amount of illumination reflected by the object in the scene. These are called the illumination and the reflectance components and are denoted by $i(x, y)$and $r(x, y)$, respectively. The two components combine as a product to form an image. The indices $x$ and $y$ are the 2-D spatial coordinates of the image scene.

$$f(x, y) = i(x, y)r(x, y) \qquad (3.1)$$

*where* $0 < i(x,y) < \infty$(3.2)

*and* $0 < r(x,y) < 1$(3.3)

Equation 3.3as a boundary condition indicates that reflectance is 0when absorption is total and 1 when reflectance is total. The nature of $i(x,y)$ is determined by the illumination source, and $r(x,y)$ is determined by the characteristics of the objects [35].

### 3.1.2 Image Description

An intensity image can be defined as a two dimensional function $f(x,y)$, where $x$ and $y$ are the spatial (plane) coordinates and the amplitude of $f$ at any pair of coordinates $(x,y)$ is called the intensity or gray level of the image at that point. When $x, y$, and the amplitude values are all finite, discrete quantities the image is called a digital image. Mathematically, such an image is represented as a$M$ by $N$ matrix. The elements of the matrix are known as picture elements, pel, or pixels. They represent the intensity of a scene at a given spatial coordinate. The following equation models a digital intensity image as a matrix.

$$f(x,y) = \begin{bmatrix} f(0,0) & \cdots & f(0,N-1) \\ \vdots & \ddots & \vdots \\ f(M-1,0) & \cdots & f(M-1,N-1) \end{bmatrix} \quad (3.4)$$

### 3.1.3 Image Sampling and Quantization

The output of most image sensors is a continuous voltage waveform whose amplitude and spectral behaviour are related to the physical phenomenon being sensed. To create a digital image, the continuous data must be transformed to become discrete and finite. This involves two process: namely, sampling and quantization. Digitizing the coordinate values (space) is called sampling while digitizing the amplitude values (intensities) is called quantization [35].

### 3.1.4 Colour Images

The colour of objects is a consequence of the nature of light being reflected by the objects. Humans and some other animals perceive colour from a limited range of electromagnetic spectrum known as visible light. If a body reflects light that is balanced in all visible wavelengths, it appears white to the observer. However, a body that favours reflectance in aparticular range of visible spectrum exhibits some shades of colour. For example, red objects reflect light with wavelengths in the range of 600nm to 700nm while absorbing most of the energy at other wavelengths. The motivation for colour image processing stems from two reasons. First, colour is a powerful object descriptor and can encode details of objects very easily and concisely. Second, humans can perceive thousands of colour shades as opposed to a few dozens of gray shades. Colours are specified by means of colour models or colour spaces.

### 3.1.5 Colour Models

Colour models facilitate the specification of colours in a standard, generally accepted way. A colour model can therefore be thought of as a coordinate system or space where each colour is represented uniquely. Most colour models are oriented either towards hardware or towards application where colour manipulation is the goal. Some of the most commonly used colour models include RGB (red, blue, green) model, CMY (cyan, magenta, yellow) model, CMYK (cyan, magenta, yellow, and black), HSI (hue, saturation and intensity) model, and HSV (hue, saturation, value) model [35,36].

## 3.2 Image Pre-Processing

The ultimate goal of image pre-processing is to make an image more suitable for subsequent computer processing. There are three main image pre-processing tasks namely: image rescaling, image restoration, and image enhancement. Image rescaling involves either reducing the image size in order to speed up processing and occupy less memory space or increasing the image size

for purposes of magnifying some image details. Image restoration involves reducing or eliminating noise from an image while image enhancement is concerned with improving the visual quality of an image.

### 3.2.1 Image Rescaling

The two commonly used methods of digital image rescaling are nearest neighbour interpolation and pixel replication. In nearest neighbour interpolation, an imaginary mesh grid is overlaid to the image to be resized. The number of grids in the mesh should be equivalent to the size of the required image. Gray levels of the original image are assigned to the new image (mesh grid) based on the nearness of the grid location to the original image pixel [35]. The other method is pixel replication. Here, adjacent columns and rows of an image are replicated or deleted to produce an image whose size is an integer number of times of the original image [35]. Pixel replication is computationally effective compared to nearest neighbour interpolation.

### 3.2.2 Image Restoration/ Image Filtering

The ultimate goal of restoration techniques is to improve an image in some predefined sense. Image restoration is an objective task. It attempts to reconstruct or recover an image that has been degraded by using a priori knowledge of the degradation phenomenon. Therefore, restoration techniques are geared towards modelling the degradation and applying the inverse process in order to recover the original image. Restoration is implemented in either the frequency domain or the spatial domain of an image by filtering [35, 36].

#### 3.2.2.1 Spatial Domain Filtering

This operation works with values of an image neighbourhood and corresponding values of a sub-image that has the same dimensions as the image neighbourhood. Commonly, the sub-image is referred to as the filter, mask, kernel, window, or template. The values of the filters are referred to as coefficients. The process of filtering, commonly referred to as convolution, involves moving the filter from point to point in an image and computing the filter response using some

predetermined relationship. The relationship may be a linear operation between the filter and the image neighbourhood such averaging (mean filtering), or a non-linear operation such as determining the median of the image neighbourhood (median filtering) [35].

#### 3.2.2.2 Mean Filtering

Mean filtering is used for reducing noise in images by averaging the image intensity between adjacent pixels. Mean filtering is implemented by replacing each pixel value by the mean value of its neighbourhood. This has the effect of eliminating pixel values which are not representative of their surroundings. Often a 3 by 3 filter kernel is used to perform mean filtering. However, larger filter kernels may be used if a more severe smoothing is required.

#### 3.2.2.3 Median Filtering

Median filter is used for removing noise while preserving useful features in an image. The filtering process is implemented by replacing each pixel value in an image by the median value of the image neighbourhood. The median value is computed by first sorting all pixel values of the image neighbourhood in numerical order. The middle value is then chosen as the median. In so doing random noise is eliminated from an image without creating a new unrealistic pixel value as may be the case for mean filtering. Therefore sharp transitions in an image such as edges are preserved in this type of filtering.

#### 3.2.2.4 Frequency Domain Filtering

Although filtering in spatial domain is equivalent to filtering in the frequency domain, the mechanics of implementingthe process in the two domains differ. In frequency domain, Fourier transforms of both the image neighbourhood and the filter are computed. The two transforms are then multiplied. An inverse Fourier transformation is then performed to the product. This becomes the response of the operation.

$$G(u,v) = H(u,v) \cdot F(u,v) \quad (3.5)$$

$$Filtered\ Image = \mathcal{F}^{-1}[G(u,v)] \quad (3.6)$$

where: $H(u, v)$ is the Fourier transform of the filter.

$F(u, v)$is the Fourier transform of the image.

### 3.2.3 Image Enhancement

The goal of image enhancement is to make an image visually appealing to a human observer. This is a subjective area since the viewer is the ultimate judge of how well a particular method works. A number of image enhancement techniques exist. These include intensity transformation, histogram matching, and histogram equalization amongst others [35, 36].

## 3.3 Image Segmentation

Image segmentation involves partitioning a digital image into its constituent regions. The goal of image segmentation is to locate objects and boundaries (lines and curves) in an image. Each of the pixels in a given object in an image share similar characteristics with other pixels belonging to the same object (set). These characteristics include; colour, texture, size, orientation, intensity, connectivity etc.

Several image segmentation algorithms and techniques exist. The most commonly used include; morphological image segmentation methods, thresholding based on image histograms, edge detection methods, region growing, and split-and-merge methods [35 - 40].

### 3.3.1 Morphological Image Segmentation Methods

Morphology signifies form or structure. In image processing, mathematical morphology is used as a means of identifying and extracting image descriptors based on properties of form or shape within the image. The key areas of application are segmentation together with automated counting and inspection. The language of mathematical morphology is set theory. Sets in mathematical morphology represent objects in an image. For example, the set of all white pixels in a binary image is a complete morphological description of the image. In binary images, the sets in question are members of 2-D integerspace $Z^2$, where each element of a set is a tuple (2-D vector) whose

coordinates are (x,y) coordinates of a white (or black, depending on the convention) pixels in the image. Gray scale digital images can be represented as a set whose components are in $Z^3$. In this case, two components of each element of the set refer to the coordinates of a pixel, and the third component corresponds to the discrete gray-level value. Sets in higher dimensional spaces can contain other image attributes, such as colour and time varying components.

#### 3.3.1.1 Binary Images: Foreground, Background and Connectedness

A binary image is an image in which each of the pixels assumes one of the only two possible discrete, logical values, 1 or 0. Pixels in binary images having local value 1 are referred to as the image foreground pixels, while those pixels having logical value 0 are called image background pixels. An object in a binary image consists of any group of connected pixels. Two definitions of connections are commonly used. If it is required that the foreground pixel must have at least one neighbouring foreground pixel to the north, south, east, or west of itself to be considered as part of the same object, then we are using 4-connection. If however, a neighbouring foreground pixel to the north-east, north-west, south-east, or south-west is significant for it to be considered as part of the same object, then we are using 8-connection.

Binary images have no textural content. Thus, the only property of interest in binary images is shape, size and location of the objects in the image. The effect of morphological image processing in binary images reduces simply to the determination of which foreground pixels becomes background and which background pixels become foreground [34].

Generally, whether or not a given foreground or background pixel has its value changed depends on three things. Two of them are the image and the type of morphological operation carried out. The third factor is the structuring element (SE) and is a key factor in any morphological operation. The structuring element is the entity which determines exactly which image pixels surrounding the given foreground/background must be considered in order to make the decision to change its value or not. The choice of a particular structuring element is central in image processing [3]. A structuring element can have an arbitrary size and shape.

### 3.3.1.2 Dilation and Erosion

These operations are fundamental to morphological processing. Many of the morphological algorithms are based on these primitives.

### 3.3.1.3 Binary Image Dilation

If A is a binary image and B the structuring element, dilation of A by B, denoted A⊕B is defined as

$$A \oplus B = \{z|\left(\hat{B}\right)_z \cap A \neq \emptyset\} \quad (3.7)$$

This equation is based on obtaining the reflection of B denoted as $\hat{B}$ about its origin and shifting this reflection by z. The dilation of A by $\hat{B}$ then is the set of all displacements, z, such that $\hat{B}$ and $A$ overlap by at least one element. Based on this interpretation we may write equation (3.7)as

$$A \oplus B = \{z|\left(\hat{B}\right)_z \cap A \subseteq A\} \quad (3.8)$$

This operation is implemented by successively placing the centre pixel of the structuring element on each background pixel, if any of the neighbourhood pixels are foreground pixels, then the background pixel is switched to foreground. An application of dilation is bridging gaps in binary images, that is, filling unwanted holes (backgrounds) surrounded by a foreground region. The technique can also be used to enlarge an image [35, 37].

### 3.3.1.4 Binary Image Erosion

As before, if we let A to represent a binary image and B the structuring element, then the erosion of A by B, denoted as A⊖B, is defined as

$$A \ominus B = \{z|B_z \subseteq A\} \quad (3.9)$$

This equation is implemented by successively placing the centre pixel of the structuring element on each foreground pixel. If any of the neighbouring pixels are background pixels, then the foreground pixel is switched to background pixel. One simple application of erosion is elimination of irrelevant details (in terms of size) from a binary image [35,37].

### 3.3.1.5 Opening and Closing

Opening is the name given to the morphological operation of erosion followed by dilation with the same structuring element. We denote the the opening of A by structuring element B as A∘B, and is defined as

$$A \circ B = (A \ominus B) \oplus B \qquad (3.10)$$

The general effect of opening is removal of small isolated objects from the foreground of an image, placing them in the background. It tends to smooth the contour of binary objects and break narrow joining regions in an object [35, 37].

Closing is the name given to morphological operation of dilation followed by erosion with the same structuring element. The closing of A by B is denoted as A·B, and is defined as

$$A \cdot B = (A \oplus B) \ominus B \quad (3.11)$$

Closing tends to remove small holes in the foreground, changing small regions of background into foreground. It tends to join narrow isthmuses between objects [35,37].

### 3.3.1.6 Other Morphological Operations

Other useful morphological operations can be derived from the basic dilation and erosion operations. These operations include: boundary extraction, region filling, hit or miss transform, morphological thining and opening by reconstruction and many more [35, 37].

#### 3.3.1.7 Gray Scale Erosion and Dilation

The same principals of mophological processing can be extended to intensity images. Just as in binary case, the building blocks of gray scale morphology are the fundamental operations of erosion and dilation.

The gray scale erosion of an image A by structuring element B is denoted A⊖B and the operation may be described as the process of successively placing a structuring element B over each location in the image A and for each location a minimum value of A-B occurring within the local neighbourhood defined by the structuring element is obtained.Gray scale dilation of image A by structuring element B is denoted by A⊕B and is implemented in a similar way to gray scale erosion except that instead of taking the minimum of the difference between A and B in the neighbourhood defined by B, the maximum value of sum of A and B in the neighbourhood is taken [37].

#### 3.3.1.8 Morphological Gradient

This is implemented by taking the difference of morphological dilation and erosion using the same structuring element, i.e.

$$g = (f \oplus b) - (f \ominus b) \quad (3.12)$$

As expected, morphological gradient highlights sharp gray level transitions in the input image. Morphological gradient obtained using symmetrical structuring element tends to depend less on the edge directionality.

### 3.3.2 Histogram Based Segmentation

This approach aims at grouping pixels into clusters having similar properties. For example, an object may be segmented from the background by defining a threshold value, T, such that all pixels having intensity values less than T belong to the background and those pixels values greater than T are foreground.

Often the correct threshold value is obtained using image histogram. An image histogram is a distribution of gray levels of an intensity Image. Often in an image histogram, there are two or more modes. These correspond to different regions of the image. A good threshold value is located near the "valley" bordering two adjacent modes. Two commonly used algorithms for computing threshold values are Otsu method [38] and Zack's algorithm [39].

#### 3.3.2.1 Otsu Threshold Technique

In this algorithm, the process starts by a selection of an initial estimate of a threshold value,$T$. Segmenting the image using $T$ will produce two groups of pixels;$G1$, consisting of all pixels with gray values greater than $T$and $G2$, consisting of pixels with values less than or equal to T. The average gray level value μ1 and μ2 for the pixels in region $G1$ and $G2$ is computed and a new threshold value T is obtained as follows

$$T = \frac{1}{2}(\mu 1 + \mu 2) \quad (3.13)$$

The above procedure is repeated until the difference in $T$ in successive iterations is smaller than a predefined parameter $T_0$ [36, 38].

#### 3.3.2.2 Zack's Algorithm

In this technique, the threshold value is set by constructing a line from the highest point, h([$b_{max}$]) of a gray level image histogram, h([b]), to the lowest point h([$b_{min}$]). Perpendicular distance, d between the line and the histogram values is computed. The threshold value is chosen as the intensity value $b_o$ where the maximum distance, d, intersects the gray level axis of the histogram [39]. Figure 3.1 illustrates the process.

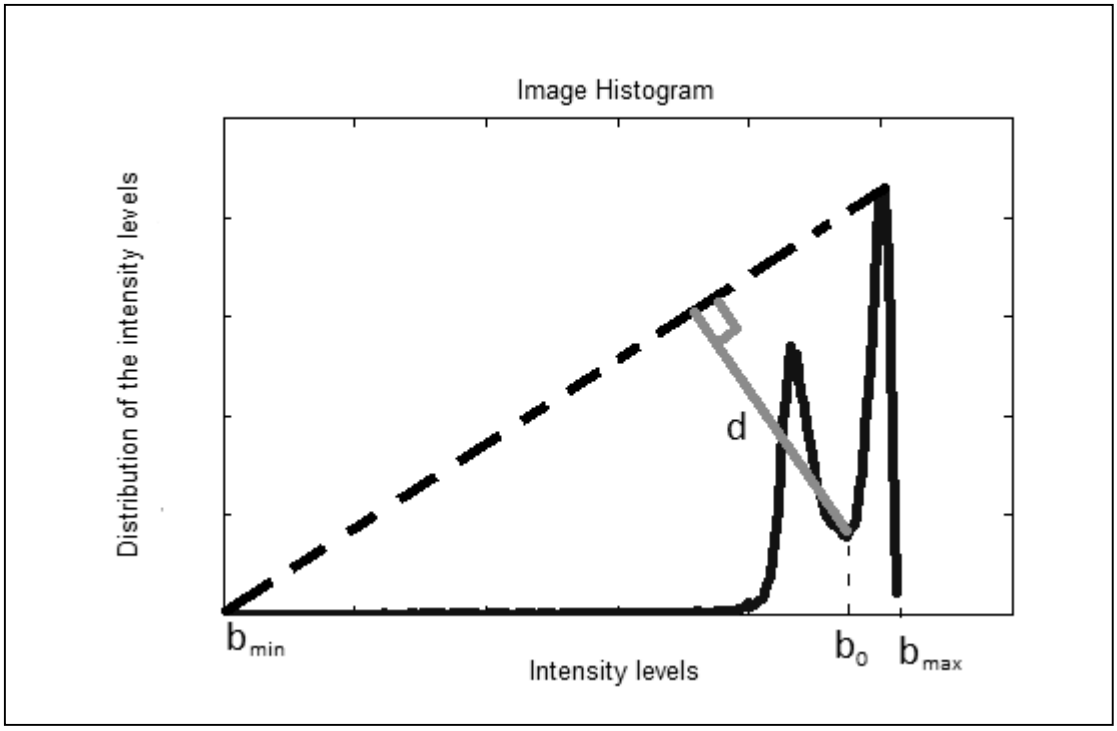


**Figure 3.1: Graphical description of Zack's algorithm**

## 3.4 Feature Extraction

After an image has been segmented, the resulting aggregate of segmented pixels usually is represented and described in a form suitable for further computer processing. Representing and describing regions involves two choices. An object can be represented and described in terms of its external characteristics (its boundary) or in terms of its internal characteristics (the pixels comprising the region). After a representation scheme has been chosen, useful data is extracted from the object based on the chosen representation. For example an object can be represented in terms of its boundary and the boundary described by features such as length, orientation, boundary signature, etc.

An external representation is chosen when the primary focus is on shape characteristics. An internal representation is chosen when the primary focus is on the regional properties, such as colour and texture. Sometimes both internal and external descriptors are used for more accurate description of an object. The features selected as descriptors should be as insensitive as possible to variation in size, translation, and rotation.

### 3.4.1 Boundary Based Representation and Description

Here objects are represented in terms of their external features – which are basically the shape and size of the boundary. Some of the features commonly used to describe boundaries of objects include, chain code, polygonal approximation, shape number, boundary signatures, and Fourier descriptors [35 - 37]. A boundary signature is the representation of a 2D boundary as a 1D function. This is done by computing the centroid of a given shape and plotting the distance from the centroid to the boundary $r$ as a function of polar angle $\Theta$. The signature of a closed boundary is a periodic function, repeating itself on an angular scale of $2\pi$. Thus, one simple and neat way of representing and describing a closed boundary is through a 1-D (radial) Fourier expansion. The signature can be expressed in real and complex form as follows:

$$r(\Theta) = \frac{a0}{2} + \sum_{n=1}^{\infty} a_n cos(n\theta) + \sum_{n=1}^{\infty} b_n sin(n\theta) \quad \text{(Real form)} \tag{3.14}$$

$$r(\theta) = \sum_{n=-\infty}^{\infty} c_n exp(in\theta) \quad \text{(Complex form)} \tag{3.15}$$

The shapes can then be encoded by Fourier expansion coefficients which are easily calculated through use of the orthogonalityrelations of Fourier series [37].

### 3.4.2 Regional Based Representation and Description

In this approach the internal (surface) characteristics of the object pixels are sought. Some of these descriptors include form factor which is a shape metric, roundness which gives the degree of roundness of an object, aspect ratio which gives the proportion of length to width of an object, solidity which gives the proportion of the object which is filled, extent which is a measure of elongation, compactness, and convexity. These features are summarized in the Table 3.1:

**Table 3.1: Some common, single-parameter descriptors for approximate shape in 2-D [36].**

| Descriptor | Definition | Circle | Square | Rectangle as $\frac{a}{b} \to \infty$ |
|---|---|---|---|---|
| Form factor | $\frac{4\pi * Area}{perimeter^2}$ | 1 | $\pi/4$ | - > 0 |
| Roundness | $\frac{4 * Area}{\pi * maximumDiameter^2}$ | 1 | $2/\pi$ | - > 0 |
| Aspect ratio | $\frac{Maximum\ Diameter}{Minimum\ Diametre}$ | 1 | 1 | - >∞ |
| Solidity | $\frac{Area}{Convex\ Area}$ | 1 | 1 | - > 0 |
| Extent | $\frac{TotalArea}{Area\ of\ Bounding\ Rectangle}$ | $\pi/4$ | 1 | Indeterminate |
| Compactness | $\frac{\sqrt{4 * Area}/\pi}{Maximum\ Diameter}$ | 1 | $\sqrt{2}/\pi$ | - > 0 |
| Convexity | $\frac{Convex\ Perimeter}{Perimeter}$ | 1 | 1 | 1 |

### 3.4.2.1Statistical Moments

The concept of moments forms an important part of elementary probability theory. If we have a probability density function p(x) which describes the distribution of the random variable x, the n[th] moment is defined as:

$$m_n = \int_{-\infty}^{\infty} x^n p(x) dx \quad (3.16)$$

The zero[th] moment $m_0 = \int_{-\infty}^{\infty} p(x) dx$ gives the total area under the function p(x), and is always equal to unity if p(x) is a true probability density function. The first moment $\mu = m_1 = \int_{-\infty}^{\infty} xp(x) dx$ corresponds to the mean value of the random variable. The central moments of a function describe the variation about the mean and are defined as:

$$m_n = \int_{-\infty}^{\infty} (x - \mu)^n p(x) dx \quad (3.17)$$

The most common central moments, $m_2 = \int_{-\infty}^{\infty}(x-\mu)^2 p(x)dx$ is well known as variance and forms the basic measure of how spread out the density function is. Higher order moments can yield other information on shape of the density function, such as skewness (tendency to shoot further on one side of the mean than the other side).

Moments extend naturally to 2D (and higher dimensional) functions. Thus, the pq$^{th}$central moment of a 2D density function $p(x,y)$ is given by:

$$m_{pq} = \iint_{-\infty}^{\infty}(x-\mu_x)^p(y-\mu_y)^q p(x,y)dx\,dy \tag{3.18}$$

We calculate the moments of images, however, by replacing the density function with intensity image $I(x,y)$ or, a corresponding binary image, $b(x,y)$. The intensity image is thus viewed as an un-normalized probability density function which provides the probability of a particular intensity occurring at location $(x,y)$.For a binary image, the moments directly encodes information about the shape. If $I(x,y)$ is a digital image, then Eq. 3.16becomes

$$m_{pq} = \sum\sum(x-\mu_x)^p(y-\mu_y)^q I(x,y) \tag{3.19}$$

Where, the summation is taken over x and y. Central moments are translational invariant. In general, however, we require shape descriptors to be scale and rotation invariant as well. The pq$^{th}$ normalized central moment is defined as:

$$n_{pq} = \frac{m_{pq}}{m_{00}^{\beta}} \tag{3.20}$$

*where*, $\beta = \frac{p+q}{2} + 1$ and $p + q \geq 2$.

From these normalized central moments, it is possible to calculate seven derived quantities which are invariant to translation, scale and rotation [35, 37]:

$$\emptyset_1 = n_{20} + n_{02}$$

$$\emptyset_2 = (n_{20} - n_{02})^2 + 4n_{11}^2$$

$$\emptyset_3 = (n_{30} - 3n_{12})^2 + (3n_{21} - n_{03})^2$$

$$\emptyset_4 = (n_{30} + n_{12})^2 + (n_{21} + n_{03})^2$$

$$\emptyset_5 = (n_{30} - 3n_{12})(n_{30} + n_{12})[(n_{30} + 3n_{12})^2 - 3(n_{21} + n_{03})^2] + (3n_{21} - n_{03})(n_{21} + n_{03})[3(n_{30} + n_{12})^2 - (n_{21} + n_{03})^2]$$

$$\emptyset_6 = (n_{20} - n_{02})[(n_{30} + n_{12})^2 - (n_{21} + n_{03})^2] + 4n_{11}(n_{30} + n_{12})(n_{21} + n_{03})$$

$$\emptyset_7 = (3n_{21} - 3n_{03})(n_{30} + n_{12})[(n_{30} + 3n_{12})^2 - 3(n_{21} + n_{03})^2] + (3n_{21} - n_{30})(n_{21} + n_{03})[3(n_{30} + n_{12})^2 + (n_{21} + n_{03})^2] \quad (3.21)$$

#### 3.4.2.2 Texture

An important approach to region description is to quantify its texture content. Surface features which can be described by texture include smoothness, coarseness, and regularity. The three principal approaches used in image processing to describe the texture of a region are statistical, structural, and spectral [35]. Statistical approaches yield characterizations of texture such as smooth, course, grainy etc. Structural techniques deal with the arrangement of image primitives, such as the description of texture based on regularly spaced parallel lines. Spectral techniques are based on properties of Fourier spectrum and are used primarily to detect global periodicity in an image by identifying high energy, narrow peaks in the spectrum.

#### 3.4.2.3 Statistical Approaches

Statistical moments of the gray-level histogram of an image or region can be used to describe the texture. If $z$ is a random variable denoting gray levels and $p(z_i)$, $i = 0,1,2,\ldots,L-1$, is the corresponding histogram, where L is the number of distinct gray levels, the nth moment of z about the mean is defined as

$$\mu_n(z) = \sum_{i=0}^{L-1}(z_i - m)^n p(z_i) \quad (3.22)$$

Where $m$ is the mean value of z (the average gray level):

$$m = \sum_{i=0}^{L-1} z_i p(z_i) \quad (3.23)$$

The second moment (variance,$\sigma^2(z) = \mu_2(z)$) is of particular importance in texture description. It is a measure of gray level contrast that can be used to establish descriptors of relative smoothness. For example the measure:

$$R = 1 - \frac{1}{1+\sigma^2(z)} \quad (3.24)$$

is zero for area of constant intensity (the variance is zero there) and approaches 1 for large values of $\sigma^2(z)$.

The third moment is defined as,

$$\mu_3(z) = \sum_{i=0}^{L-1}(z_i - m)^3 p(z_i) \quad (3.25)$$

and is a measure of skewness of the histogram while the fourth moment is a measure of the histogram's flatness. The fifth and higher order moments are not so easily related to histogram shape, but they do provide further quantitative discrimination of texture content. Other useful texture measures based on histograms include a measure of "uniformity", given by:

$$U = \sum_{i=0}^{L-1} p^2(z_i) \quad (3.26)$$

And an average entropy measure, which measures variability and is zero for constant images

$$e = -\sum_{i=0}^{L-1} p(z_i) log_2 (p(z_i)). \quad (3.27)$$

### 3.4.2.4 Spectral Approach

Spectral texture approach is useful for quantifying the difference between periodic and non-periodic texture patterns. This approach is based on the Fourier transform, which is suited for describing directionality of periodic and non-periodic 2 dimensional patterns in an image.

#### 3.4.2.5 Structural Approach

This is a qualitative way of expressing structural relationships of objects present in an image. Different objects are assigned values referred to as shape numbers based on their shapes. The number of digits in a shape number gives the order of the shape number and its value limits the number of possible different shapes an object can take. Given any two objects, degree of similarity, $k$, is defined as the largest order for which their shape numbers coincide. This metric can be used to compare similarity of different objects in image or in comparison of objects in an image and a give template.

## 3.5 Object Recognition

One of the objectives of image processing is recognition of objects present in an image. The key to successful object recognition lies in selection of appropriate descriptive features of an image. Pattern recognition can be categorized into two principal areas: decision-theoretic and structural [33]. The first category deals with patterns described using quantitative descriptors, such as length, area and texture. The second category deals with patterns best described by qualitative descriptors such as chains, trees, nets and other structural primitives.

Decision theoretic approaches to recognition are based on the use of decision (or discriminate) functions. Let $\boldsymbol{x} = (x_1, x_2, \dots x_n)^T$ represent an n-dimensional pattern vector. For W pattern classes $w_1, w_2 \dots w_n$, the basic problem in decision-theoretic pattern recognition is to find W decision functions $d_1(\boldsymbol{x}), d_2(\boldsymbol{x}), \dots d_w(\boldsymbol{x})$ with the property that, if a pattern **x** belongs to class $w_i$, then

$$d_i(\boldsymbol{x}) > d_j(\boldsymbol{x}) \text{for } j = 1,2 \ \dots \dots \dots W \tag{3.28}$$

In other words, the unknown pattern is said to belong to the $i^{th}$pattern class if upon substitution of **x** into all decision functions, $d_i(\boldsymbol{x})$ yields the highest numerical value [35]. Some of the techniques for classification falling under this category iclude, minimum distance classifiers, matching by correlation, Bayes classifier, support vector machine and neural networks [35]. Image correlation

is of little practical significance since the technique is not invariant to scaling and rotation of an image. In practice, minimum distance classifier works well when the distances between the means of the different classes is large compared to the spread or randomness of each class with respect to it mean. However, simultaneous occurrence of large mean separations and relatively small class spread occurs rarely in practice. Bayes classifier as an example of a statistical classifier works on the principle of minimizing the total average loss of misclassifying a vector pattern. In order do this, the probability density functions of the patterns in each class, as well as the probability of occurrence of each class, must be known. This is the limitation of this method since often the statistical properties of the pattern classes are unknown.

### 3.5.1 Artificial Neural Networks (ANN)

In situations where statistical properties of pattern class are not known, classification of a decision theoretic problem is best handled by methods that yield the required decision functions directly via training. Neural network is one such approach. It comprises of inter-connections of nonlinear computing elements organized as networks reminiscent of the way neurons are believed to be interconnected in the brain. The basic block of a neural network comprises of a computing element where weighted inputs are added followed by a nonlinear activation element which receives the sum of the weighted inputs and gives an output value. This basic architecture of artificial neural network is referred to as the perceptron. They consist of a single layer of neurons. Perceptrons can learn linear decision functions that separate two linearly separable training sets. Figure 3.2 shows schematically the model for two pattern classes.

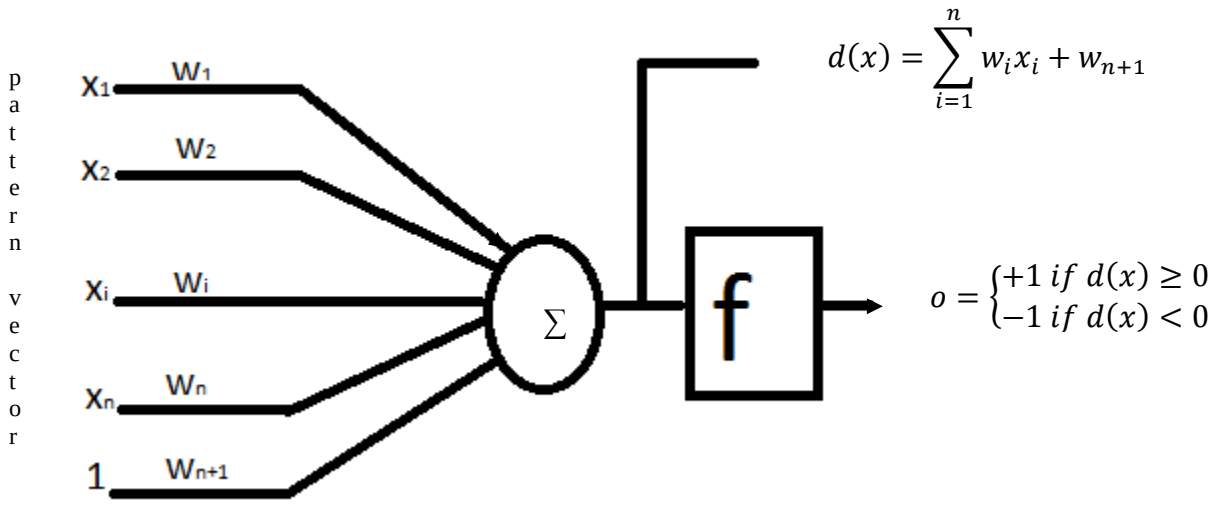


**Figure 3.2: The neuron model, it consists of the weighted inputs, the summer, and the activation function f.**

The response of the device is based on a weighted sum of its inputs; that is

$$d(x) = \sum_{i=1}^{n} w_i x_i + w_{n+1} \quad (3.29)$$

This is the linear decision function with respect to the components of the pattern vectors. When $d(\boldsymbol{x}) > 0$ the threshold element causes the output of the perceptron to be, $+1$, indicating that the pattern **x** was recognized as belonging to class $w_1$. On the other hand, when $d(\boldsymbol{x}) < 0$, x is classified as belonging to $w_2$. If n such neuron models are arranged into a layer, they can be used to classify patterns into $2^n$ pattern classes, provided the classes are linearly separable [40]. The limitation of a perceptron is that that it cannot classify classes of patterns whose decision functions are not linearly separable. To solve this problem, use is made of multilayer neural networks. There are two classes of multilayer neural networks namely, feed-forward networks and feedback networks. The feed – forward ANNs allow signals to travel one way only; from the input to output. There are no feedback loops and so the output of any layer is not affected by previous output of the same layer. Feed-forward networks associate inputs with output and are extensively used in

pattern recognition. Feedback network have signals travelling in both directions by introducing loops in network.

### 3.5.1.1 Learning Rule

A learning rule is a procedure for modifying the weights and biases of a network. Learning rules can be classified under three categories namely; supervised learning, unsupervised learning, and reinforcement learning.

In supervised learning, the networkis provided with a training set, which is a set of examples which give proper network behaviour: $\{p_1, t_1\}$, $\{p_{2,} t_2\}$,.....,$\{p_{Q,} t_Q\}$, where $p_Q$ is the $Q^{th}$ network input and $t_Q$ is the corresponding network output commonly referred to as the target. As the inputs are applied to the network, outputs are compared to the target. The learning rule is then used to adjust the weights and biases of the network in order to minimize the difference between the network outputs and the targets.

In unsupervised learning, the weights and the biases are modified in response to the network inputs only. There are no target outputs available. The algorithm performs some kind of clustering operation. Inputs are categorized into finite number of classes.

In reinforcement learning, the learning algorithm is provided with the network inputs and a grade (also called score). The grade is a measure of the network performance over some sequence of output.

### 3.5.1.2 Artificial Neural Network Architecture

Often a single neuron even with multiple inputs as shown in figure 3.2 is insufficient. Therefore in most cases more than one neuron connected in either one or more layers.

### 3.5.1.3 Single Layer Networks

Figure 3.3shows a single layer neural network commonly referred as the perceptron. Here there are *R* inputs, {$P_1$, $P_2$,…., $P_R$} and a row of *S* neurons. Each input is multiplied by a weight,$w_{i,j}$ and connected to every neuron. The $i^{th}$ subscript of the weight denotes the neuron which the$j^{th}$ input is connected to.

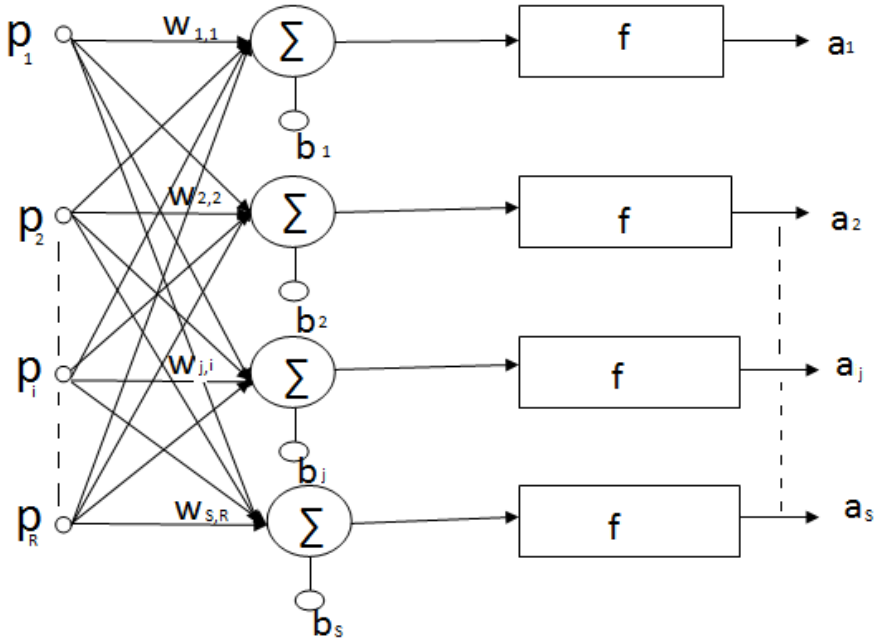


**Figure 3.3: A Layer of Neurons, $w_{j,i}$is the weight of the ith input to the jth neuron and $b_j$ is the bias of the jth neuron.**

From figure 3.3, a weight matrix for the network can be formed as shown in equation (3.30).

$$W = \begin{bmatrix} w_{1,1} & \cdots & w_{1,R} \\ \vdots & \ddots & \vdots \\ w_{S,1} & \cdots & w_{S,R} \end{bmatrix} \quad (3.30)$$

From equation (3.30), vector, $_iw$composed of the elements of the $i^{th}$ row of W can be formed as follows;

$$ {}_iW = \begin{bmatrix} w_{i,1} \\ w_{i,2} \\ \vdots \\ w_{i,R} \end{bmatrix} \quad (3.31) $$

The weight matrix can therefore be partitioned as

$$ W = \begin{matrix} {}_1W^{\mathrm{T}} \\ {}_2W^{\mathrm{T}} \\ \vdots \\ {}_SW^{\mathrm{T}} \end{matrix} \quad (3.32) $$

Therefore the $i^{th}$element of the network output vector can be written as

$$ a_i = f(n) = f\left( {}_iwp + b_i \right) \quad (3.33) $$

where$p$ is a vector of the input features.

A single neuron perceptron can classify input vectors into two categories, since its output can be either 0 or 1. Therefore the transfer function, f used is a hard limiting function (hardlim), and the output of the transfer function can be written as

$$ a_i = f(n) = hardlim\left( {}_iwp + b_i \right) = \begin{cases} 1 \; if \; n \geq 0 \\ 0 \; if \; n < 0 \end{cases} \quad (3.34) $$

Table 3.2outlines the algorithmic steps of adjusting the weights $w$, for a single neuron network with bias $b$ until the network converges to the correct weight values. The MATLAB ™ implementation of the steps is given in Appendix A.13.

**Table 3.2: Algorithmic steps for updating weights and biases for a single neuron network**

1. Pick a random value for the bias $b$, and weight $w$(the value of b is not confined to any range)
2. For every input $p$, Implement equation 3.34
3. Evaluate the error of the network using the following equation

   $e = t - a$ where $t$ is the desired network output and $a$ is the network output
4. Adjust the weight $w$ as follows

$$w^{new} = w^{old} + ep \tag{3.35}$$

$$b^{new} = b^{old} + e$$

5. Iterate the above for all the inputs and targets

Equation 3.35 is known as the perceptron rule for updating weights for a single neuron. The rule can be generalized for multiple neuron perceptron. To update the i$^{th}$ row of the weight matrix, equation 3.35 takes the following form;

$$w_i^{new} = w_i^{old} + e_i\, p \tag{3.36}$$

$$b_i^{new} = b_i^{old} + e_i$$

# CHAPTER 4: METHODOLOGY

The goal of this work was to develop a system for diagnosing malaria using microscopic images of stained blood samples. This being an image recognition and classification task, a systematic sequence of events was followed to achieve the objective. Generally, the procedure followed in solving such a problem is as follows. First an image is acquired and pre-processed, it is then segmented into different regions and appropriate features extracted. Next, a suitable classifier is used to categorize the features into their different classes. Finally, a decision is made about the information conveyed by the image based on the classes of features found by the classifier.

A similar criterion was used in this study to develop an algorithm for detection, classification and quantification of *Plasmodium* parasites. Thin blood smear images were acquired from two sources; Kenya Medical Research Institute (KEMRI) [41], and Centre for Disease Control (CDC) website [42]. The samples obtained were accompanied by their test results indicating the parasites life stages and species. KEMRI samples contained only one species of malaria (*Plasmodium falciparum*).

Microscopic images of KEMRI samples were captured using a LEICA ICC50 RGB digital camera (with a maximum camera resolution of 1600X1600 pixels) fitted on the ocular lens of a LEICA DM500 microscope available at the Department of Veterinary Medicine, University of Nairobi. A blank glass slide image was also captured and used as a reference sample. The captured images spatial resolution was automatically set to 300 by 300 pixels by the microscope software. To correct for non-uniform illumination in the KEMRI thin blood smear images, the absolute difference of KEMRI images and the blank sample image was performed. This is a standard procedure done to eliminate the effect of the sample being unevenly illuminated by the microscope's light source.

Images from CDC are posted to the website for either confirmation of diagnosis or archiving from laboratories all over the world. The *Plasmodium* life stages and species are specified for each image obtained from the website. These images are of different visual quality i.e. the images vary in their intensity contrast, hue, and magnification. This is a consequence of different techniques

used in sample preparation, image capturing and processing. Correction for non-uniform illumination was expectedto have been performed to these images since this is a standard practice.

This chapter is divided into three broad sections; the process model, diagnosis system design methodology, and classification algorithms for *Plasmodium* parasites detection, stages and species identification as well as parasitemia estimation.In the process model, a general outline of malaria diagnosis scheme is presented. This scheme is then used in the diagnosis system design methodology to evaluate different techniques available for implementing a system for diagnosing malaria. Test results for the options explored in this section are compare and decisions made on the choice of the best techniques. In the next section, classification algorithms for *Plasmodium* parasites detection, stages and species identification as well as parasitemia estimation are developed. A complete malaria diagnosis system is then presented based on the developed algorithms.

Test results of the malaria diagnosis system developed in this chapter are presented and discussed in chapter 5. The performance of this system is compared to the results given by expert microscopists from KEMRI and CDC. A discussion of the main findings, strengths and limitations of this work is also given.

## 4.1 The Process Model

Here, a process model for malaria diagnosis was developed. This model was supposed to take thin blood smear images as its input and give correct malaria diagnosis. Therefore a top-down design approach was adopted in realizing the model. Figure 4.1 gives an overview picture of the mode.


**Figure 4.1: Black box model of malaria diagnosis system**

The above model was implemented using three main processes, namely; image processing, image classification and parasitemia estimation as show in the block diagram of figure 4.2.

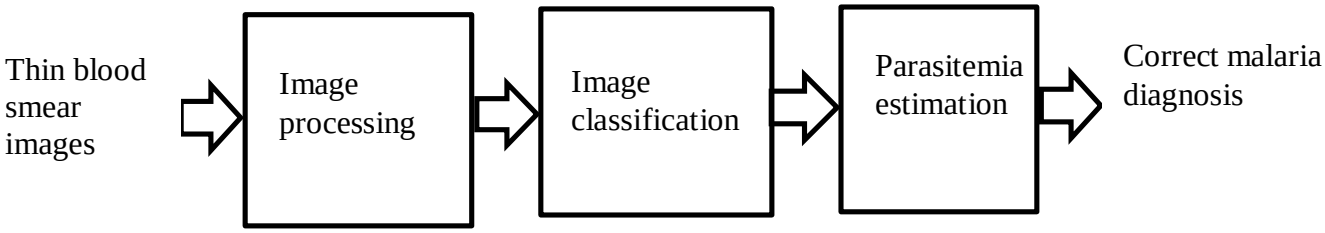


**Figure 4.2: The main processes of the malaria diagnosis system**

Image acquisition entails capturing of thin blood smear images using an optical microscope fitted with a digital camera. After images are captured they are loaded to a computer where they are processed. Processing involves the following stages. Image resizing, noise reduction, segmentation of both erythrocytes and *Plasmodium* parasites and feature extraction. Finally, the extracted features are taken to trained classifiers where diagnosis is made by determining whether the image is infected or not. If an image is found infected, *Plasmodium* parasite life stage and species are determined. The degree of infection (parasitemia estimation) is a process which can be carried out after image classification. Depending on the information being sort for, it can be determined after detection of infection or classification of the parasites stages or species. Figure 4.3 depicts the refined process model of the malaria diagnosis system with all the stages involved.

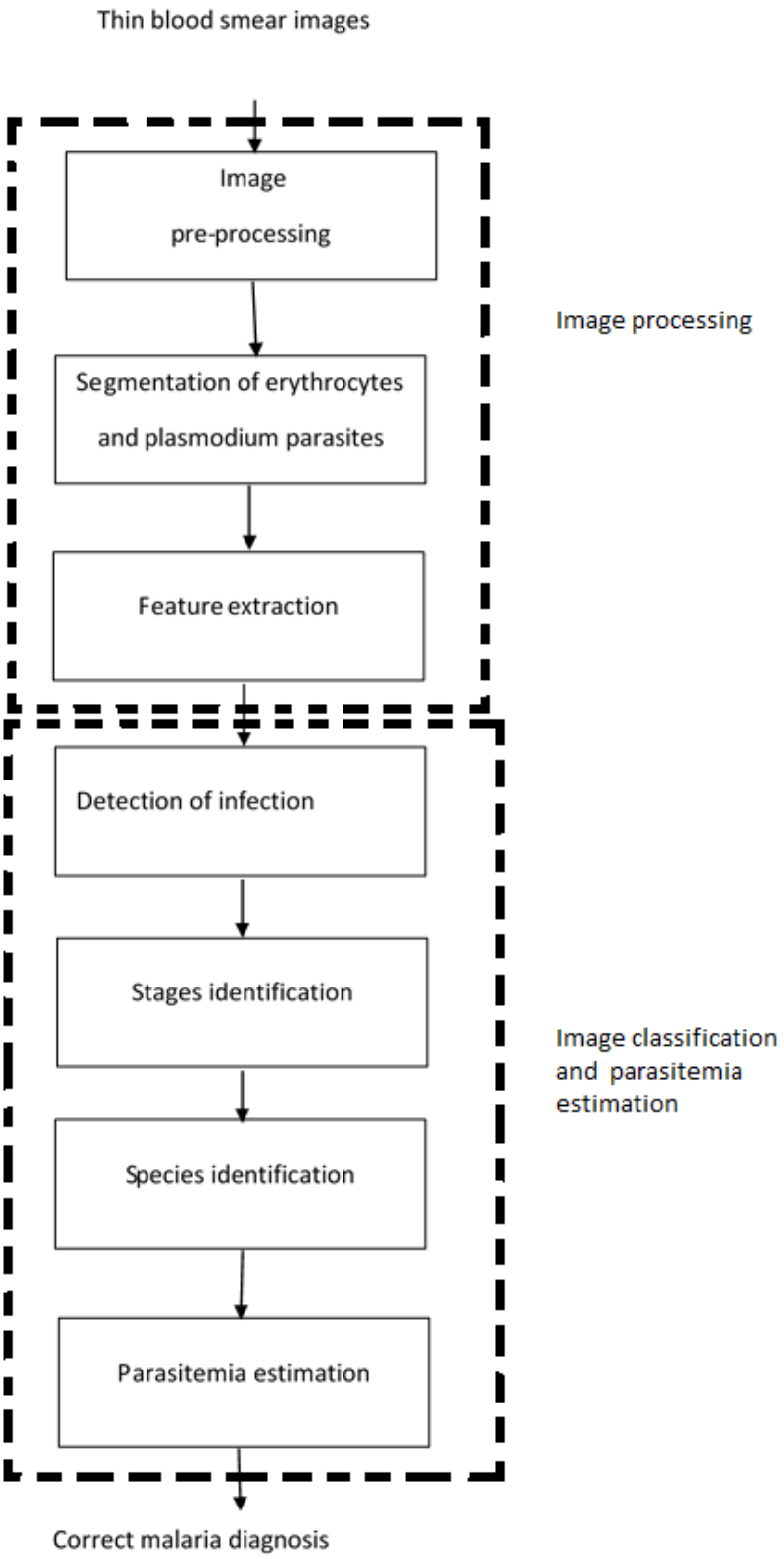


**Figure 4.3: Refined model of the malaria diagnosis system**

## 4.2 Diagnosis System Design Methodology

Careful consideration of every step involved in the algorithm development was taken in order to achieve an efficient and reliable malaria diagnosis system. This section presents a discussion of the design issues involved. A comparison is made of the feasible options available for developing an algorithm for detection and classification of *Plasmodium* parasites. Decisions on the best techniques to choose in designing the malaria diagnosis system are then made based on the test results obtained.

### 4.2.1 Image Pre-Processing

The goal of this step was to make the acquired images more suitable for subsequent processes - mainly image segmentation and feature extraction. Basically, there are three main objectives for image pre-processing. One is to resize the image for the purposes of either magnifying the image through digital zooming, or reducing the image size in order to speed up processing. The second objective of image pre-processing is to reduce or eliminate noise from the acquired image. Third is to enhance the image contrast for visual evaluation.

In this case, digital zooming and contrast enhancement were not necessary since the task of image classification and recognition was to be performed by a computer and not a human operator. However, size reduction was necessary in order to have all images with uniform size proceeding to the next stage. Images from CDC were of different spatial resolution with 300 by 300 square pixel images being the smallest of all. KEMRI images had their size normarlized to 300 by 300 square pixels by the microscope software.

Noise reduction was also considered to reduce some undesirable effects in the images which often are acquired during the process of sample preparation and image acquisition such a non-uniform illumination, salt and pepper noise and image blurring. Filtering operation using a square median filter was performed to both images from CDC and from KEMRI. This operation served to remove spurious noise present in the images. The length of the median filter used was 5 by 5, a value obtained from the previous related work of Ross *et al*[30]. After filtering, HSI imagesof the corresponding images were computed and stored. This was motivated by the fact that HSI colour

spaces can easily highlight some parasite information which is difficult to identify in RGB colour space [32].

#### 4.2.1.1 Image Size Reduction and Noise Reduction

In order to develop a standard algorithm to process images from both sources, all images were rescaled to have the same size. Since no enlargement was needed for KEMRI images, the size of their spatial resolution (300 by 300 pixels) which corresponded to the minimum size of CDC images was adopted to be the standard image size of the pre-processed images. Filtering operation using a median filter was performed to the rescaled images from both sources to reduce noise in the images. Table 4.1 gives the algorithmic steps involved in this stage. These steps have been implemented in MATLAB$^{TM}$ in Appendix A.1.

**Table 4.1: Pre-processing steps for KEMRI and CDC images**

1. Load a sample image, $Is$ and specify it source, either KEMRI or CDC.
2. Perform median filtering using a 5 by 5 square filter to $Is$
3. Determine the spatial resolution $Is$
4. If the image size is greater than 300 square pixels, resize the image by a scale factor of sf where $sf = \frac{300}{minimum(imagelength,imagewidth)}$
5. Determine the centre coordinates, $(x_o, y_o)$ of the resulting image and use it to crop a subset of the image using the following parameters;

   $Topleftcoordinates = (x_o\text{-}150\ , y_o - 150)$

   $widthoftheimagetobecropped = 300$

   $heightoftheimagetobecropped = 300$

   $$Is = crop(Is, [x_o - 150, y_o - 150,300,300])$$

6. Create a copy of the resized image and convert it into HSI colour space.

#### 4.2.1.2 Test Results for Image Size Rescaling

Figure 4.4 shows two images from CDC and KEMRI before and after size rescaling. Figure 4.4a is an image from CDC whose size is 1600 by 1600 pixels while figure 4.4b is an image captured from KEMRI blood samples. Figure 4.4c and 4.4d gives the resultant images after image rescaling operation.

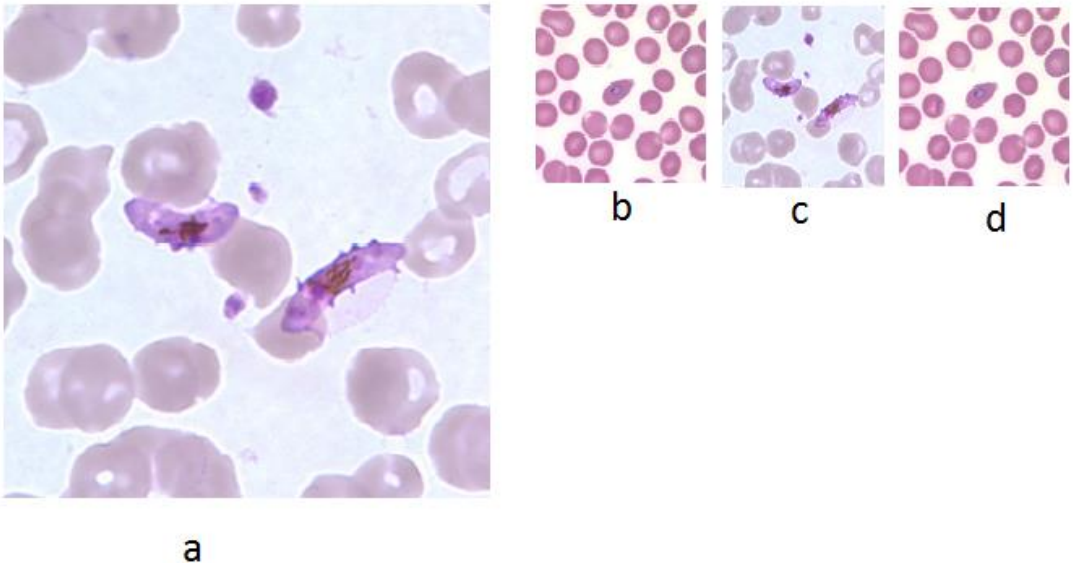


**Figure 4.4: Test results of image rescaling, a. CDC image, b. KEMRI image, c. and d. rescaled CDC and KEMRI images respectively**

After image rescaling CDC image size reduced to 300 by 300 pixels while maintaining its useful features such as erythrocytes, parasites and background regions. The KEMRI image size remained the same after rescaling. This therefore confirmed that the image rescaling algorithm given in Table 4.1 produced the desired results of rescaling images from both KEMRI and CDC to the same spatial resolution. Image rescaling was necessary to speed up computation in the subsequent stages especially in feature extraction stage and image segmentation and classification of *Plasmodium* parasites by artificial neural network. These two tasks are time consuming since computation is performed on every image pixel location.

#### 4.2.1.3Test Results for Noise Reduction

The effect of image filtering using median filtering and compensation of non-uniform illumination (in the case of KEMRI images) described in the algorithmic steps in Table 4.1 was investigated. Here, both the raw images and pre-processed images of figure 4.4 were segmented using Zack's algorithm (refer to theoretical background and diagnosis system design methodology for details of this technique). The test results of the segmentation process are presented in figure 4.5.

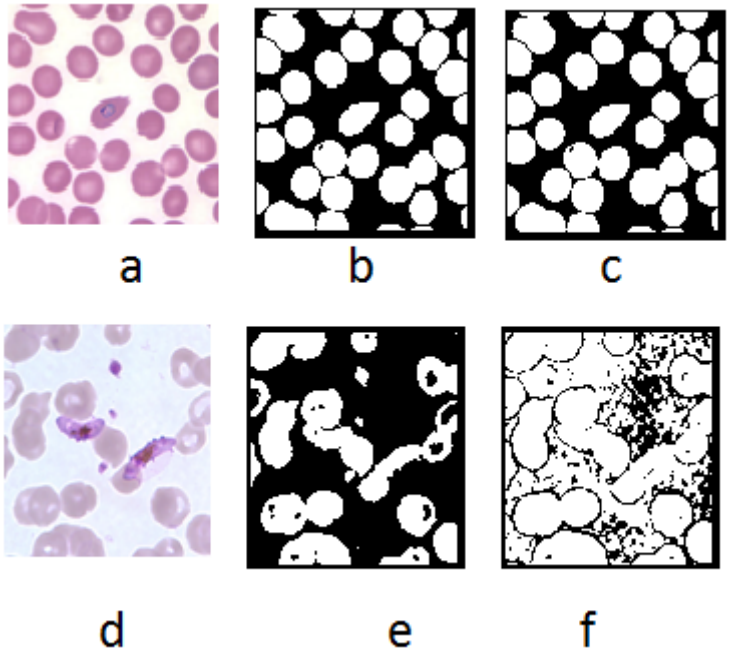


**Figure 4.5: Effect of image filtering, a. and d. pre-processed KEMRI and CDC images, b. and e. binary images obtained from the pre-processed images, c. and f. binary images obtained from raw images from KEMRI and CDC respectively.**

Figure 4.5***a*** and ***d*** are the rescaled KEMRI and CDC images respectively. Erythrocytes of these images were segmented before and after performing the filtering operation with a median filter. From the results it can be seen that for KEMRI image, there is no notable difference in the two binary images. However, for CDC image segmenting the image after the filtering operation resulted to a significant improvement of the binary image quality. This could be as a result of CDC images being degraded by noise, an effect that is corrected by median filtering. Some of the possible sources of such noise include unbalanced illumination of the sample in the microscope, poor sample preparation, sample degradation or a combination of these factors. By performing

median filtering random noise also referred to as salt and pepper noise was smoothed and this led to an improvement in the quality of the segmented binary image.

## 4.2.2 Image Segmentation

There were two objectives of image segmentation. One was to isolate individual erythrocytes from the rest of blood constituents and the second was to partition *Plasmodium* parasites from the infected erythrocytes. Two image segmentation schemes were explored and their results compared. One was the traditional image segmentation technique of histogram thresholding and the other was the use of artificial neural network for image segmentation.

### 4.2.2.1 Erythrocyte Segmentation by Histogram Thresholding

Both RGB and HSI images were used for segmentation. For RGB images, the green component was used. This is because the green colour component is the least noisy of RGB components and parasites are most visible [30]. For HSI colour space, both hue and saturation components were used for segmentation.

Histograms of these gray scale images were obtained and their threshold values determined by implementing Otsu's algorithm. The algorithmic steps for erythrocyte segmentation is given in the Table 4.2, and implemented in MATLAB$^{TM}$ in Appendix A.2.

**Table 4.2: Algorithmic stepsfor Erythrocyte segmentation**

1. Load a preprocessed sample image to be segmented
2. Obtain the corresponding HSI image of the sample,
3. Obtain the green component image from RGB images and hue and saturation components from HSI images
4. Use Otsu's algorithm to segment erythrocytes in the green, hue and saturation component images.
5. Determine the coordinates of bounding rectangles enclosing every object.

#### 4.2.2.2 Test Results for Erythrocyte Segmentation Using Histogram Segmentation

Histograms of sampled images from CDC and KEMRI were obtained and their threshold values determined using Otsu's algorithm. The algorithmic steps of Table 4.2 are implemented in MATLAB$^{TM}$ in Appendix A.2. Test results of erythrocyte segmentation using image histogram are presented in figure 4.6 and figure 4.7 for a CDC image and a KEMRI image respectively.

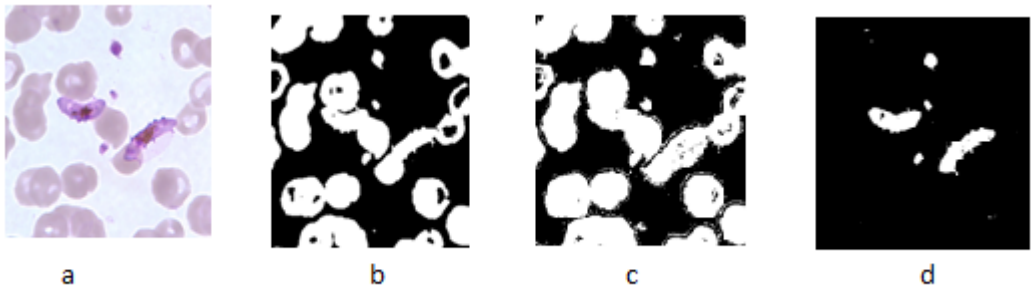


**Figure 4.6: CDC image histogram thresholding, a) pre-processed image from CDC, b), c), and d) resultant binary images obtained from thresholding the green, hue, and saturation component images.**

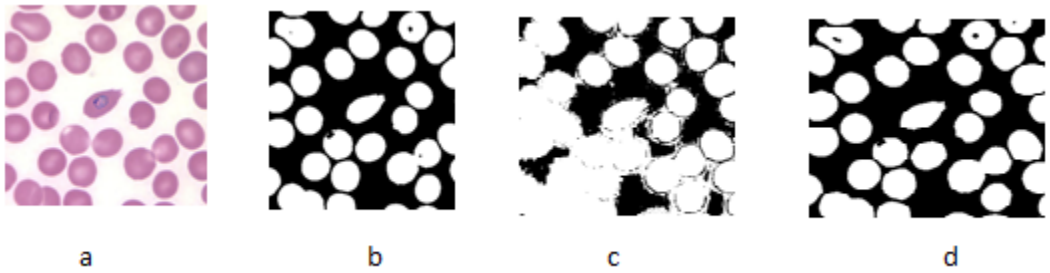


**Figure 4.7: KEMRI histogram thresholding, a) pre-processed image from KEMRI, b), c), and d) resultant binary images obtained from thresholding the green, hue, and saturation component images**

For CDC image, the green component image produced good segmentation results for erythrocytes but it also captured the *Plasmodium* parasite regions as part of the foreground. The hue component resulted to a binary image whose foreground (erythrocyte regions) had noisy boundaries. The saturation component failed to produce erythrocytes as the objects but instead segmented the parasites.

The same test was conducted with a KEMRI image to determine which colour component image would produce the best erythrocyte segmentation results. Figure 4.7 shows the KEMRI image, and the resulting binary images from its corresponding green, hue, and saturation image colour components. It can be observed from the Figure 4.7 that the binary images from green component of RGB images and saturation component image produced good erythrocytes regions but as in the case of CDC image, hue component image produced a noisy binary image.

From these observations, it was deduced that the green colour component of RGB image is the most suitable for segmentation using histogram segmentation techniques. This is in agreement with the findings of Di Rubertoet *al.*, [33] that the green colour component is the least noisy. This could be due to the quantum efficiency of the camera being optimum at the green wavelength.

#### 4.2.2.3 Training of Artificial Neural Network

ANN is asupervised learning technique used to classify patterns into different classes based on a training set among other modelling capabilities. Training an ANN involves supplying the network with input features and their corresponding targets (desired outputs). The network then tries to adjust its input coefficients (commonly referred as the weights and biases) until a point where its output matches the corresponding target for a given input feature. When this happens the network is said to have learnt to classify different classes of input features. A trained ANN is capable of correctly classifying features which it has not been trained with. This is known as network generalization.

MATLAB$^{TM}$ has a toolbox for creating artificial neural networks. This toolbox divides input features into three groups. The first group is the training set and is made of 60% of the network inputs. It is used in training the network (adjusting the weights and the biases). The second and the third groups each consist of 20% of the network inputs. One group is used for validating the network. This means checking that the network is generalizing and it stops training before over-fitting. The other group is used as an independent test of the network generalization.

#### 4.2.2.4 Artificial Neural Network Segmentation of Erythrocytes

In this method, a multilayer neural network was trained to partition the image into two regions; erythrocytes region and the image background. Two sets of feature vector were used to train the network. One set comprised of RGB pixel values and the other set comprised of both RGB and HSI image pixel values. The features were divided into two classes; erythrocytes and the background pixel values. A total of 540 feature vectors were used to train the neural network, with 340 feature vectors belonging to the erythrocytes class and 192 feature vectors belonging to the background class.

#### 4.2.2.5 Test Results for Artificial Neural Network Segmentation of Erythrocytes

Erythrocyte segmentation using two ANN classifiers were tested. The first classifier was trained with only pixel values of RGB images. The other classifier was trained with both RGB and HSI image pixel values. Table 4.3 gives the classification accuracy in percentage attained by the two ANN classifiers.

**Table 4.3: Performance of erythrocyte segmentation using ANN classifiers**

| Feature vector used | Training session (%) | Validation session (%) | Test session (%) | Overall performance (%) |
|---|---|---|---|---|
| **RGB features vectors only** | **100** | **100** | **100** | **100** |
| **RGB and HSI features** | **100** | **99.9** | **100** | **99.9** |

From the results given in Table 4.3, the performance of the two ANN classifiers was impressive (above 99%). However, the network trained only with RGB features performed marginally better than the one trained with both RGB and HSI features. This can be attributed to the fact that neural network classification accuracy decreases when the number of features is increased while the sample size is held constant [46 - 47]. It can be concluded that RGB features are adequate to distinguish erythrocytes from the rest of the thin blood smear image using an ANN.

The Artificial Neural Network trained with RGB features was used to segment the same images used in histogram segmentation, one from KEMRI and the other from CDC. The binary images of Figure 4.8 (b and d) were obtained. From these images it can be observed that the ANN managed to capture the erythrocyte regions well in both CDC and KEMRI images. Figure 4.8 indicates that ANN managed to produce fairly good segmentation results for the erythrocytes for both CDC and KEMRI images. The quality of the segmented images is comparable with that obtained by histogram segmentation using the green colour component of the images.

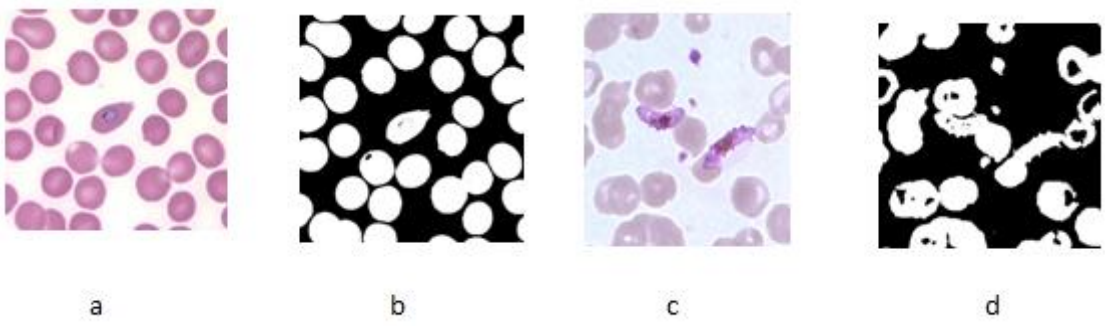


**Figure 4.8: Erythrocyte segmentation results of Artificial neural network, a) is the pre-processed image from KEMRI, c) is the pre-processed image from CDC, b) and d) are the resultant binary images obtained as the outputs of ANN trained to segment erythrocytes.**

#### 4.2.2.6 Plasmodium Parasite Segmentation

This stage served two purposes; the first was detection of *Plasmodium* parasites and the second was identification of parasites locations to extract suitable features from, to aid in stages, species and parasitemia determination. Just as in the case of erythrocytes segmentation, there were two options available for segmenting the images for *Plasmodium* parasites; the conventional image processing segmentation techniques and the adaptive machine learning technique of training a classifier to isolate parasite occupied regions from the rest of the image constituents.

In the first option, histogram segmentation was the method of choice as it partitions an image into different regions based on the presence of objects rather than boundaries of the regions occupied

by objects. This is desirable because the staining process of blood smears on glass slides highlights surface features of *Plasmodium* parasites and makes them easier to identify. Other region based segmentation techniques such as split and merge and region growing are computationally demanding and callfor prior knowledge of the image to be segmented such as average intensity, variance of intensity in a given neighbourhood etc. Such information would be difficult to specify given the fact that images used, especially from CDC, were of varied quality.

#### 4.2.2.7 Segmentation of Plasmodium Parasites Using Image Histogram

Histograms of the green component of the RGB images were used to segment the parasites. The green component was chosen since it produced the better regional segmentation results than other colour components belonging to RGB and HSI components (refer to the section on erythrocyte segmentation). The threshold value used to segment the gray scale image was determined by a modified Zack's algorithm. Zack's algorithm just like Otsu's algorithm is designed to locate the global minimum points in an image histogram. This point becomes the threshold value for separating foreground objects from the image background. Often the global minimum of a blood image is the point separating the image background and the erythrocytes. This is due to the fact that the two dominant modes in these image histograms correspond to background and erythrocyte pixel value. The mode due to *Plasmodium* parasites pixels is negligible compared to the above two modes. Therefore, a global minimum would separate erythrocytes from the image background and not the parasites.

To segment parasite regions, Zack's algorithm was modified to locate local minimum which corresponds to the boundary between parasite regions and the rest of the blood constituents. First, a histogram, $h$of a gray scale image (in this case the green component RGB image) was determined. Then a global minimum point, of the histogram was sought using either the original Zack's algorithm or Otsu's method. Then, a matrix of 1 by 256 (the total number of gray levels in the intensity image) elements was formed. The first values of the matrix elements were set to ones and the rest were set to zeros. This matrix was multiplied element by element with histogram $h$ to form a modified histogram. A global minimum point of the new histogram was used as the threshold value for segmenting *Plasmodium* parasites from rest of the image constituents. Table

4.4 summarizes the algorithmic steps for implementing the modified Zack's algorithm. MATLAB$^{TM}$ code for the described steps can be found in Appendix A.4 while the test results obtained upon implementing the algorithm are presented in the next sub-section.

**Table 4.4: Algorithmic steps for implementing modified Zack's algorithm**

1. Extract the green component image, from the RGB image
2. Find the histogram $\boldsymbol{h}$, for this gray scale image
3. Use Otsu's method to determine the global minimum point $\boldsymbol{T}$, of the histogram
4. Form a 1 by 256 matrix $\boldsymbol{M}$, with the first $\boldsymbol{T}$ elements as ones and the rest as zeros
5. Multiply matrix $\boldsymbol{M}$ with histogram $\boldsymbol{h}$ element by element to form a 1 by 256 matrix $\boldsymbol{hh}$ , i.e.,

$$\boldsymbol{hh} = \boldsymbol{h}^{\boldsymbol{T}}.\boldsymbol{M}$$

6. Apply Zack's algorithm to determine the global minimum point, for the histogram $\boldsymbol{h}$
7. Use to threshold

#### 4.2.2.8 Test Results of Segmentation of Plasmodium Parasites Using the Modified Zack's Algorithm

Segmentation of *Plasmodium* parasites in images of thin blood smears using a modified version of Zack's algorithm was tested. Two images randomly selected one from KEMRI and the other from CDC were segmented using the Zack's algorithm technique modified to detect parasite regions. Figure 4.9 shows the original images alongside the binary images obtained after segmentation.

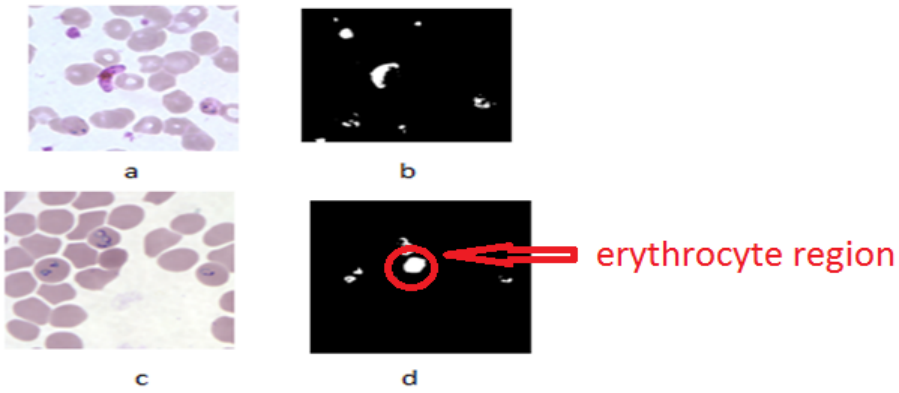


**Figure 4.9: *Plasmodium* parasite segmentation using a modified Zack's algorithm, a. KEMRI image, c. CDC image, b. and d. the corresponding binary images of the parasites.**

As seen in Figure 4.9, the algorithm produced a fairly good segmentation result for the *Plasmodium* parasites in KEMRI image (a) but miss-classified an erythrocyte as a parasites in the CDC image (c) in the region circled in red (d). The histogram technique classified an erythrocyte as a parasite due to the fact that the misclassified erythrocytes intensity levels were lower compared to other erythrocytes. One limitation of this technique is that it does not take into account the hue information of the objects to be segmented and therefore segmentation is done on the bases of the magnitude of the gray scale value of the image pixels. This technique is also prone to high rates of false positive cases likely to arising from the algorithm misclassifying artefacts as *Plasmodium* parasites. This problem can be solved using a segmentation technique that utilizes the full colour information in addition to the intensity values of an image.

#### 4.2.2.9 Segmentation of Plasmodium Parasites Using Artificial Neural Network

In this method, two multilayer neural network classifiers were trained to identify *Plasmodium* parasites from the rest of the image constituents. One network was trained using a feature vector formed from corresponding pixel values of the red, green and blue image colour components of both CDC and KEMRI images. The second network was trained using feature vectors formed from the red, green, blue, hue, saturation, and intensity components of the RGB and its corresponding HSI colour images.

#### 4.2.2.10 Test Results for Artificial Neural Network Segmentation of Plasmodium Parasites

Two sets of feature vectors were used to train two artificial neural network classifiers to segment *Plasmodium* parasites from the rest of the blood constituents. The two sets were, a three dimensional feature vector consisting of pixel values for red, green and blue image colour components and a six dimensional feature vector consisting of pixel values of red, green, blue, hue, saturation and intensity colour components. The performances of these two networks are presented in Tables 4.5.

**Table 4.5: ANN Performance in detection of*Plasmodium* parasite**

| Feature vector used | Training session % accuracy | Validation session % accuracy | Test session % accuracy | Overall performance % accuracy |
|---|---|---|---|---|
| **RGB features vectors alone** | **100** | **99.9** | **99.9** | **99.9** |
| **Combined RGB and HIS features** | **93.5** | **88.6** | **36.2** | **82.4** |

From these results, ANN trained with RGB features performed better than the one trained with both RGB and HSI features. The overall performance of the networks trained with RGB features was 99.9% while the performance for the network trained with both RGB and HSI features was significantly lower (82.4%).Besides, the second classifier performed poorly in generalizing as can be seen from the test plot which attained mere 36.2% accuracy.The reason for lower classification accuracy by the ANN trained with both RGB and HSI feature as compared to the one trained with RGB features only is the fact that when the feature size was increased, keeping the sample size constant, the classification accuracy decreased. A similar observation was noted previously in segmentation of erythrocytes using ANN. This can be attributed to the fact that ANN performance depends on the number of training examples and the size of the feature vectors. If the dimension of the feature vector is increased, the number of training examples should also be increased for the network performance to improve [46 - 47]. Therefore since the number of training examples was the same for both networks the performance of the network trained with more features did not

translate to improved classification accuracy. Using ANN trained with RGB features, *Plasmodium* parasites were segmented from the two images used previously in histogram segmentation technique (see Figure 4.9*a*and *c*). The results are presented in Figure 4.10.

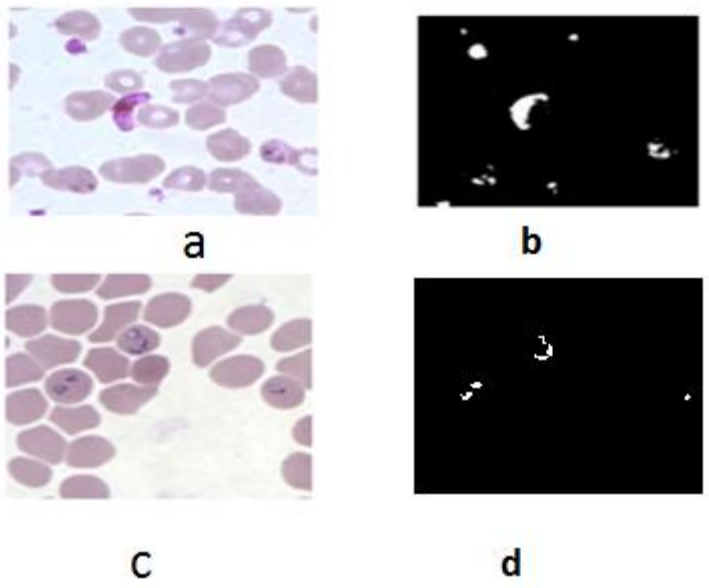


**Figure 4.10: ANN *Plasmodium* parasites segmentation; *a*and *c*: pre-processed KEMRI and CDC images respectively, b and d: their corresponding binary images of *Plasmodium* parasites.**

As can be seen from Figure 4.10 b and d, the neural network classifier managed to segment *Plasmodium* parasites correctly for both KEMRI and CDC images. Figure 4.10 d shows that the network correctly detected regions infected with *Plasmodium* parasites and didn't miss-classify erythrocytes as parasites as was the case in histogram segmentation. This indicates that ANN trained with RGB features can segment erythrocytes and *Plasmodium* parasites more accurately than histogram thresholding. Therefore this technique was adopted in the diagnosis system.

### 4.2.3 Classification of *Plasmodium* Parasite Stages and Species

Automation of *Plasmodium* parasites classification into their respective stages and species using RGB images of thin blood smears is a challenging task due to the high correlation of parasite features in different stages and species. This makes it very difficult to develop a mathematical

model of categorizing the parasites respective stages and species. Based on this complexity, neural network classifiers were considered to be the best tools for the task since they can be trained to perform classification of different stages and species using examples of image features of infected and non-infected erythrocyte images [30, 32]. Therefore no prior statistical information of the training set is need.

#### 4.2.3.1 Stages Classification

Two sets of features were used to train the neural network classifiers to classify *Plasmodium* life stages. The first one was, direct pixel values of RGB. This choice was motivated by the fact that artificial neural network classifiers trained with RGB features produced good performance in the previous test results (refer to the section on erythrocyte and *Plasmodium* parasite segmentation).

The algorithmic steps used for this procedure are given in Table 4.6. The MATLAB$^{TM}$ code for feature extraction is given in Appendix A.6.The artificial neural network was designed and trained using the steps described in Table 4.6 and their performance noted.

**Table 4.6: Algorithmic steps for stages identification using colour information**

1. Load an RGB image whose *Plasmodium* parasites stages is to be determined
2. Convert the image into double class.
3. Extract the red, green, and blue intensity pixel values for different parasite stages
4. Repeat step 3 above for several images
5. Form feature vectors of three elements from the three colour components extracted in step 4
6. Categorize these features into four classes; trophozoites, schizonts, gametocytes and band/basket stages.
7. Form the corresponding target (desired output) values for feature classes of step 6
8. Train a multilayer neural network with varying numbers of hidden neurons and record learning accuracies.

9. Stop training mean the mean square error between the targets and the network output is minimum

The second technique explored for *Plasmodium* parasites stages differentiation was the use of the parasites morphological, colour and texture information. Here, another set of features comprising of morphological (shape and size), colour and texture features were extracted. These are the features used by human microscopists to distinguish between stages and species of *Plasmodium*.

Once an erythrocyte had been classified as infected from the previous stage, the parasite size, shape, texture, number of nucleated objects per infected erythrocyte, and their separation distances were evaluated. Besides colour information was also represented in form of the average hue, saturation, intensity, red, green, and blue components of the infected erythrocytes. These parameters were then used as feature vector for training a multilayer neural network to classify *Plasmodium* parasites into its respective life stages. To avoid over-fitting, training was stopped when the highest value of correlation coefficient for the testing session was achieved. The algorithmic steps used for this classification task are given in Table 4.7. The MATLAB$^{TM}$ code for implementing these steps is given in Appendix A.7.

**Table 4.7: Algorithmic steps for *Plasmodium* parasites stage classification using colour, morphological and texture information.**

1. Use ANN trained to segment *Plasmodium* parasites from infected erythrocytes to obtain binary images of *Plasmodium* parasites
2. Use ANN trained to segment erythrocytes to obtain binary images of infected erythrocytes
3. Determine the following features from the segmented objects which represent the parasites;
    i. Ratio of the parasite area to area of the infected erythrocyte
    ii. The seven moment invariants of both the colour and binary images

4. Use the intensity and saturation components of infected erythrocyte to determine the following features
    i. R-measure
    ii. 3rd moment
    iii. Uniformity
    iv. Entropy
5. Form a feature vector from the features extracted above
6. Use the feature vector obtained in 5 above to train a multi-layer neural network to categorize images of infected erythrocytes into their respective life stages.
7. Use different numbers of hidden neuron while repeating step 6 above, stop straining when the correlation coefficient for testing session starts to reduce while that of validation session increase.
8. Determine the classification accuracy of the multi-layer artificial neural network.

#### 4.2.3.2 Test Results for Stages Determination

In the first ANN classifier used for stages identification, 15 images each from CDC and KEMRI were used to classify the detected *Plasmodium* parasites into their respective stages. The network was trained with a three dimensional feature vector which comprised of RGB image pixel values. The performance of the network was recorded in Table 4.8. From these results it can be seen that the network attained an overall classification accuracy of 75.5% with a generalization ability of 74.8%.

**Table 4.8: Performance of stages identification using only RGB colour features of the detected *Plasmodium* parasites**

| Feature vector used | Training session % accuracy | Validation session % accuracy | Test session % accuracy | Overall performance % accuracy |
|---|---|---|---|---|
| **RGB features vectors only** | **91.9** | **51.8** | **74.8** | **75.5** |

For the second ANN classifier, morphological, colour and texture features were extracted from the same 30 images used in the first classifier. The performance of the network was recorded in Table 4.9.

**Table 4.9: Performance of stages identification using morphological, colour and texture features of the detected *Plasmodium* parasites**

| Feature vector used | Training session % accuracy | Validation session % accuracy | Test session % accuracy | Overall performance % accuracy |
|---|---|---|---|---|
| **RGB features vectors only** | **95.93** | **99.91** | **99.76** | **90.34** |

From these results it can be seen that the network attained an overall classification accuracy of 90.34% with a generalization ability of 99.76%. This is a great improvement compared to the previous value of 75.5% obtained from ANN trained with RGB features to perform *Plasmodium* parasite identification. The reason for this improved performance is due to the fact that colour features alone are not adequate to describe *Plasmodium* parasites stages but rather additional information about the parasite morphology is required.

The improved performance of the ANN classifier trained with morphological, colour and texture features indicates that *Plasmodium* parasite stages can be represented by morphology, colour and texture of the parasites. This classification scheme for *Plasmodium* parasites was therefore adopted in the diagnosis system.

#### 4.2.3.3 Species Determination

As was the case with stages classification, species identification was experimented using two approaches. The first one was training a multilayer neural network classifier using only colour information of the infected erythrocyte, and the second scheme was to use a combination of colour, morphology, and texture features of infected erythrocyte.

In the first case a total of three features were used to form the feature vector. These were the red, green, and blue components of the infected erythrocytes. The features were divided into four classes, the four species of *Plasmodium* parasites which infect humans. A total of 205 infected erythrocyte sub-images were used to form 205 feature vectors. 80 feature vectors were extracted from *Plasmodium falciparum* infected erythrocytes, 50 feature vectors were extracted from *Plasmodiumovale* infected erythrocytes, 50 feature vectors were extracted from *Plasmodiumvivax* infected erythrocytes, while, 35 feature vectors were extracted from *Plasmodium malariae* infected erythrocytes. The feature vectors were used to train a multilayer neural network.

In the second case colour, morphological and texture information for both the detected parasites and infected erythrocytes were used to form the feature vector. The features were divided into four classes, the four species of *Plasmodium* parasites which infect humans. A total of 205 infected erythrocyte sub-images were used to form 205 feature vectors. 80 feature vectors were extracted from *Plasmodium falciparum* infected erythrocytes, 50 feature vectors were extracted from *Plasmodiumovale* infected erythrocytes, 50 feature vectors were extracted from *Plasmodiumvivax* infected erythrocytes, while, 35 feature vectors were extracted from *Plasmodium malariae* infected erythrocytes. The feature vectors were used to train a multilayer neural network. Table 4.8 gives the algorithmic steps used to extract the features and train the classifier which are implemented in MATLAB$^{TM}$ in Appendix A.8.

**Table 4.10: Algorithmic steps for training multilayer ANN for species identification**

1. For each infected erythrocyte sub-image, generate its RGB and HSI colour histograms and compute the first five statistical moments for each histogram.
2. Use RGB and HSI colour components of infected erythrocyte sub-images to compute four statistical texture measures namely;
    i. R-measure
    ii. 3$^{rd}$ moment
    iii. Uniformity
    iv. Entropy

3. Threshold the infected erythrocyte sub-image using the first threshold value, $T_1$ obtained from Zack's algorithm to produce a binary image of the infected erythrocyte and use this image to compute the following features;
   i. Infected erythrocyte relative size, $S_{if}$. This is obtained as follows;

$$s_{if} = \frac{I\_area}{I\_area - nI\_area}$$

   Where,

   $I\_area$ = the number of foreground pixels in an infected erythrocyte

   $nI\_area$ = the number of foreground pixels in a non-infected erythrocyte

   ii. First five statistical moments of the infected erythrocyte shape signature
   iii. Eccentricity of the erythrocyte
   iv. Compactness
   v. Roundness
   vi. Aspect ratio
   vii. Form factor
   viii. Solidity
   ix. Convexity
   x. Extent
   xi. Erythrocyte centroid
4. Threshold the infected erythrocyte sub-image using the second threshold value, $T_2$ obtained by zack's algorithm to produce a binary image of the potential *Plasmodium* parasite. Use this binary image to compute the following features;
   i. Relative size of the parasite. This is given by the following expression;

$$= \frac{Ap}{A.I.E}$$

where $Ap$ is the area of the parasitized region and $A.I.E$ is the total area of the infected erythrocytes.

ii. Eccentricity of the parasite
iii. Compactness
iv. Solidity
v. Convexity
vi. Aspect ratio
vii. Form factor
viii. Extent
ix. Roundness
x. Number of nucleated objects
xi. Separation distances of the nucleated objects
xii. Distances of the nucleated object from the centroid of the infected erythrocyte

5. Form a feature vector of each infected erythrocyte sub-image using features obtained from steps 1 ,2, 3, and 4 above.
6. Group these feature vectors in four categories based on the *Plasmodium* species infecting the erythrocyte
7. Train a multilayer ANN using the features of step six above as the training set.
8. Vary the number of neurons in the hidden layer of the ANN and record the performance of the resulting classifier.
9. Stop training mean the mean square error between the targets and the network output is minimum
10. Determine the best performance obtained in step 8 above. This is the classification accuracy of the ANN.

#### 4.2.3.4 Test Results for Species Identification

Classification accuracies of neural networks trained to differentiate species of *Plasmodium* parasites using two sets of features were investigated. One neural network was trained with RGB features while the other network was trained with a combination of morphological, colour and texture features. The networks performances were monitored for different number of hidden neurons and training was stopped when the network reached the optimum performance, i.e. when no further improvement in the classification accuracy of the network could be made. Table 4.11 shows the best performance attained by both networks.

**Table 4.11: ANN performance for species identification**

| Feature vector used | Training session % accuracy | Validation session % accuracy | Test session % accuracy | Overall performance % accuracy |
|---|---|---|---|---|
| **RGB features vectors alone** | **60.0** | **24.0** | **16.6** | **33.5** |
| **Combined morphological, colour and texture** | **100** | **93.2** | **96.2** | **95.9** |

The best performance was produced by the network trained with a combination of morphological, colour and texture features. This network yielded an overall classification of 95.85% with 96.23% generalization ability. This implies that for a new sample being classified by the network, there would be a 96.26% chance of correct species identification. This is a great improvement from the other network trained only with colour features. As before, the reason for this can be attributed to the fact that a combination of colour, morphology and texture features describes *Plasmodium* parasites species more precisely as compared to colour features alone. It was therefore concluded that artificial neural network for species identification trained with colour, morphological, and texture features should be adopted for development of the malaria diagnosis system.

## 4.2.4Parasitemia Estimation (Algorithm development)

Parasitemia is parameter for indicating the degree of infection by the parasites (*Plasmodium*). It can be quantified by computing the ratio of infected erythrocytes to the total number of

erythrocytes examined. In this study, the total number of erythrocytes was determined from the binary image of the segmented erythrocytes. The number of infected erythrocytes was determined from the parasite segmentation stage. Here, a morphological reconstruction [35 - 36] of the erythrocyte binary image using parasites binary image as the marker was carried out and the number of objects in the resulting image was taken to be the infected erythrocytes number. A common problem encountered in determining parasitemia is detemination of the number of erythrocytes in a cluster. In this work, template matching was applied to solve the problem. Here, a free standing erythrocyte was searched for in the erythrocyte image and its correlation with a cluster of erythrocytes was determined. The resulting image was thresheld using a threshold value of 0.5 since the value represents regions of strong correlation between the cluster and the template. The number of objects in the resultant image was taken to be the erythrocytes in the cluster.

For every infected image, binary images of erythrocytes and *Plasmodium* parasites were obtained. To determine the number of infected erythrocytes a morphological reconstruction operation was performed with the parasites binary image as the marker image and the erythrocyte binary image as the mask. Figure 4.12 shows an infected image (Figure 4.12a) alongside its mask image (Figure 4.12b), marker image (Figure 4.12c) and the resultant image (Figure 4.12d) after a morphological reconstruction process. The resultant image shows only infected erythrocytes.

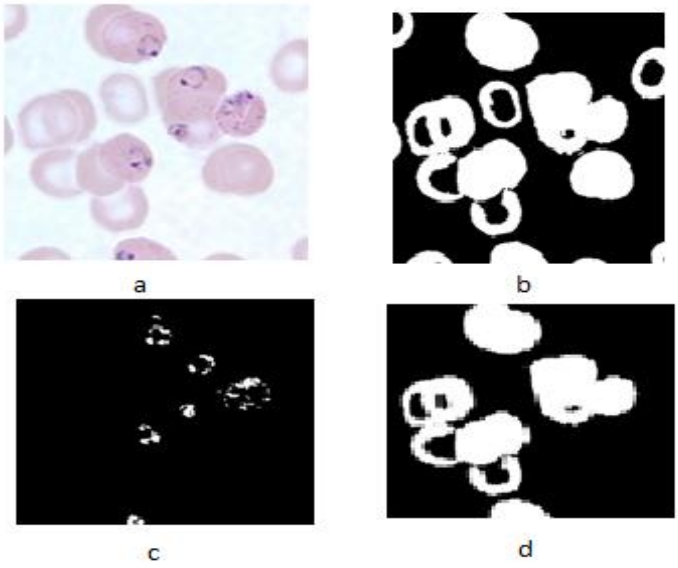


**Figure 4.11: Isolation of infected erythrocytes, a. pre-processed image, b. binary image of erythrocytes (the mask), c. binary image of the parasite (the marker), d. binary image of infected erythrocytes.**

To determinethe number of erythrocytes in a cluster, template matching between a free standing erthrocyte and the cluster was performed. As an example, Figure 4.13, shows a binary image of a cluster of erythrocytes and a template erythrocyte image. After colleration of the two, the resultant image is also shown, which is then thresheld using a threshold value of 0.5. The final image has 4 connected regions (objects). This implies that there were four erythrocyte in the cluster. This is true as can be confirmed by image in Figure 4.13(b).

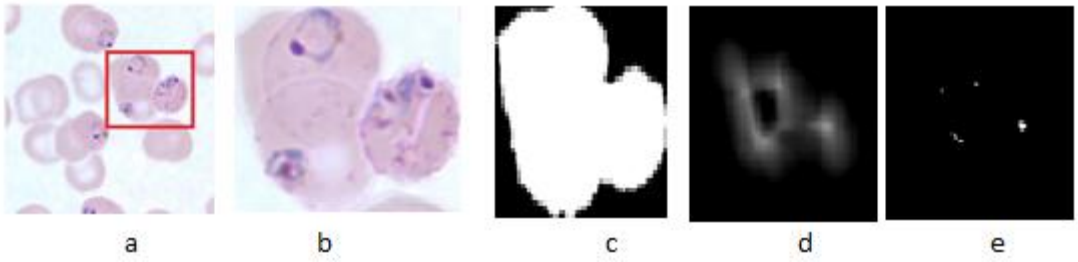


**Figure 4.12: Template matching, a) pre-processed image highlighting a cluster of infected erythrocytes, b) magnified image of the infected erythrocyte cluster, c) its binary image, c) resultant image of template matching, d) binary image indicating four erythrocytes.**

## 4.3 Algorithms for Classification and Parasitemia Estimation

In this section, algorithms for *Plasmodium* parasites detection, stages and species classification as well as parasitemia estimation are developed. A complete malaria diagnosis system which implements the algorithms is then presented.

### 4.3.1 *Plasmodium* Parasites Detection

This stage involved segmenting the pre-processed images to obtain erythrocytes and for every erythrocyte obtained, regions infected by *Plasmodium* parasites were searched for. Segmentation of erythrocytes and detection of *Plasmodium* parasites was done by multilayer neural networks using pixel values of RGB images from KEMRI and CDC. The outputs of the neural network for *Plasmodium* parasite detection was used to form a two dimensional matrix representing an image of *Plasmodium* parasites detected. This matrix was thresheld, then a morphological dilation of the binary image and a disk shaped structuring element was performed.The number of foreground

objects (in this case the parasites) was then determined. Table 4.12 gives the algorithmic steps which are implemented in MATLAB$^{TM}$ in Appendix A.10.

**Table 4.12: Algorithmic steps for *Plasmodium* parasite detection**

1. Load an image in MATLAB workspace, $I$.
2. Perform image preprocessing to get image $Ip$.
3. Segment the image to determine erythrocytes locations using ANN
4. Crop erythrocyte sub-images from image $Ip$
5. Use ANN to detect the presence of *Plasmodium* parasites in the cropped sub-images
6. Form a 2-dimensional matrix from the networks outputs
7. Threshold this matrix to form a binary image of the detected *Plasmodium* parasites
8. Perform a morphological closing of the binary image with a disk shaped structuring element to merge foreground objects close to each other

## 4.3.2 Stages Identification

Once *Plasmodium* parasites were detected from an erythrocyte, they were cropped to form a set of *Plasmodium* sub-images. Morphological, colour and texture of the image were then extracted. These features were used as inputs to a trained multilayer neural network to identify *Plasmodium* parasites life stages. Table 4.13 gives the algorithmic steps for executing the procedure.

**Table 4.13: Algorithmic steps for *Plasmodium* parasite stages identification**

1. Use the binary image obtained in step 8 of Table 4.9 to determine the shape signatures for each connected region in the image and seven moment invariants for the image
2. Determine the number of connected regions in the image
3. Determine separation distances amongst the connected regions in the image

4. Use the infected erythrocyte sub-image to compute the average intensities of the six colour components from RGB and HSI
5. Get the histogram of the green component of the infected erythrocyte sub-image and compute its five central moments
6. Form a feature vector of the parameters obtained in steps 2 to 7 above
7. Use the features vector as the input to the artificial neural network for stages identification.
8. Note the results of the ANN

### 4.3.3 Species Identification

For every infected erythrocyte, the species of the *Plasmodium* parasite infecting the cell was determined. This was done by a trained multilayer neural network using morphological, colour and texture metrics for both the parasites and the infected cell as the input features. Table 4.14is a summaryof the steps for implementing the process.

**Table 4.14: Algorithmic steps for *Plasmodium* parasite species identification**

1. For every erythrocyte found infected, crop the region infected by *Plasmodium* parasites
2. Threshold both the infected erythrocyte and the crop sub-image of the *Plasmodium* parasite using trained artificial neural networks
3. For each binary image obtained above, compute its morphological, colour and texture features as described in 2 to 7 of Table 4.10.
4. Form a feature vector of the parameters and use it as the input to the trained multilayer neural network to categorize the detected parasites into their respective species.
5. Note the output of the ANN

### 4.3.4 Parasitemia Estimation

Parasitemia was determined by dividing the number of infected erythrocytes by the total number of erythrocytes in an image. This was done by first obtaining a binary image of the erythrocytes in the image under consideration using an ANN trained to segment erythrocytes (as described in erythrocyte segmentation in diagnosis system design methodology). A single free standing erythrocyte was also searched for, cropped and segmented. This erythrocyte was used as a template. Template matching was then performed as described in parasitemia estimation in diagnosis system design methodology. The total count of erythrocytes was determined. Next, a tally was made for every erythrocyte sub-image found infected. Finally the ratio of infected erythrocytes to the total number of erythrocytes in an image was computed. This was expressed as a percentage. The algorithmic step of the process followed is given in the Table 4.15.

**Table 4.15: Algorithmic steps for parasitemia estimation**

1. Segment erythrocyte of the image under investigation using ANN for erythrocyte segmentation
2. Perform template matching of the binary image with an empirically determined erythrocyte template and determine the total number of erythrocytes in the image.
3. Tally the number of erythrocytes found infected
4. Evaluate the ratio of number of infected erythrocytes to total number of erythrocytes in the image under investigation.

## 4.4 Malaria Diagnosis System

A system detecting *Plasmodium* parasites, classifying the parasites into their respective stages and species, and determining parasitemiawas hence developed using the algorithms discussed in the previous section. This system was then tested using images from CDC and KEMRI and its results compared to those obtained by expert microscopists. The next chapter presents the system's test results. Figure 4.14is a block diagram of the developed system for malaria diagnosis.

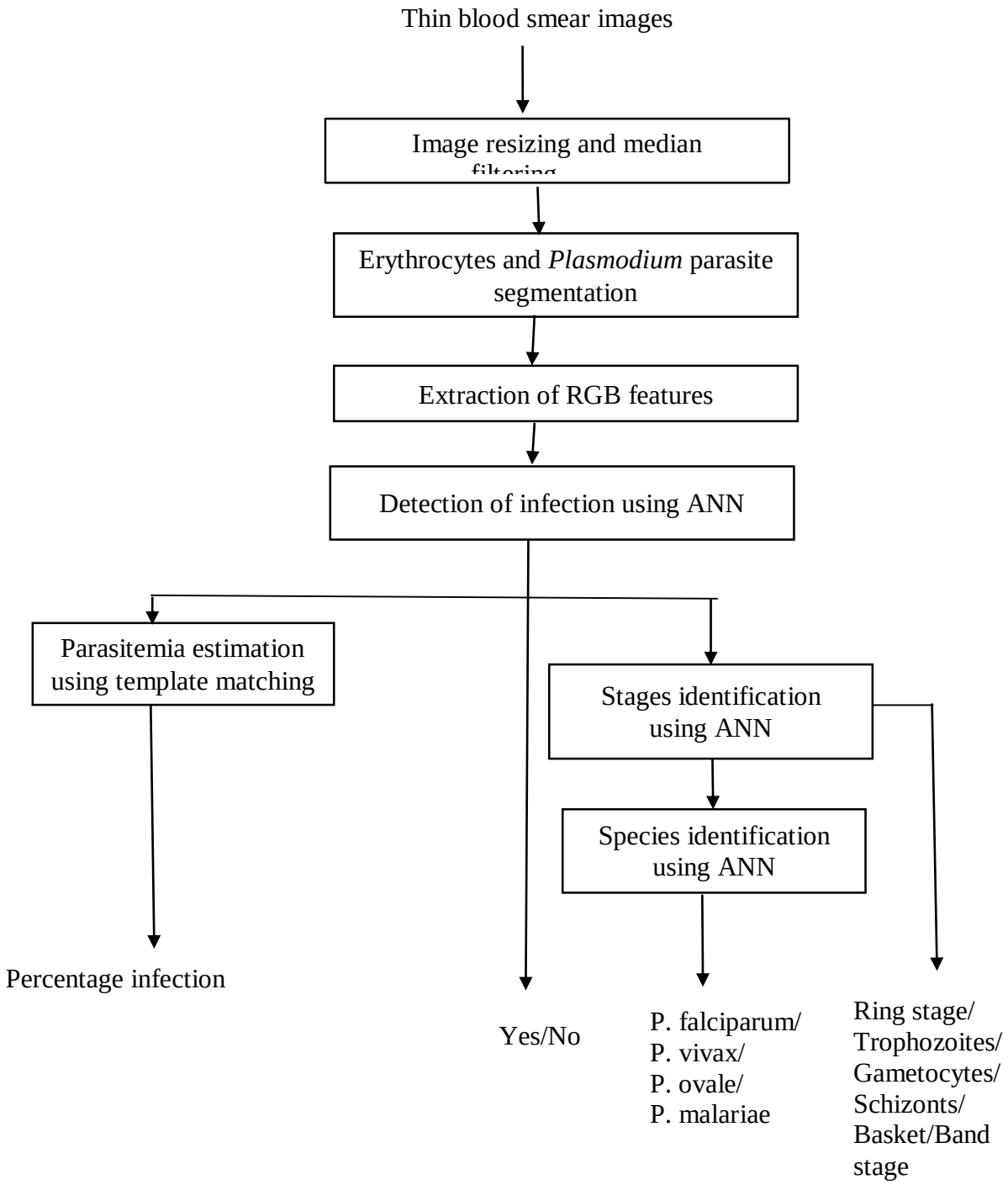


**Figure 4.13: Malaria Diagnosis System**

# CHAPTER 5: SYSTEM TESTS AND RESULTS

In this chapter, the malaria diagnosis system developed in Chapter 4 was implemented using a total of 205 images.120 images were captured from KEMRI samples while 80 were obtained from CDC online image library. From these images, a total of 305 erythrocyte sub-images were cropped. 205 sub-images comprised of infected erythrocytes while 100 images were non-infected. Images used in training of ANN classifiers were not included in this process.

The performance of the malaria diagnosis system was evaluated in four main stages: detection of *Plasmodium* parasites, classification of *Plasmodium* parasites life stages, classification of *Plasmodium* parasites species, and parasitemia estimation. In each of these four stages, the predictions made by the diagnosis system were compared to the diagnosis made by expert microscopist for validation.

## 5.1 Detection of *Plasmodium* parasites

Detection of *Plasmodium* parasites was done by a trained multilayer neural network. The network was trained with RGB colour features as this was found to be the most accurate method of detecting *Plasmodium* parasites. The network searched through the images and identified regions infected by *Plasmodium* parasites.

In order to evaluate the effectiveness of this stage, seven metrics were used. These are: True Positives (TP), True Negatives (TN), False Positives (FP), False Negatives (FN), Sensitivity,Specificity and Receiver Operating Characteristic (ROC). The TP and TN represented the number of erythrocytes diagnosed by the diagnosis system correctly either as infected or not infected. The FP represented the number of erythrocytes diagnosed by the system as infected while as they were actually not infected while FN represented the number of erythrocytes classified as not infected while they were actually infected. Detection sensitivity represented the probability of positive result given that the erythrocyte was infected and specificity represented the probability of a negative test given the erythrocyte was non-infected. The mathematical expressions of computing sensitivity and specificity of tests are given in equations 5.1 and 5.2 respectively.

$$Sensitivity = \frac{TP}{TP+FN} \quad (5.1)$$

$$Specificity = \frac{TN}{TN+FP} \quad (5.2)$$

The ROC is a metric used to check the quality of classifiers. For each class of a classifier, ROC applies threshold values across the interval (0,1) to outputs. For each threshold, two values are calculated, the True Positive Ratio (the number of outputs greater or equal to the threshold, divided by the number of one targets), and the False Positive Ratio (the number of outputs less than the threshold, divided by the number of zero targets). The area under the ROC curve (AUC) is used to access the accuracy of the classifier. A value of AUC close to 1 indicates good classification accuracy and a value close to zero indicates poor performance by the classifier.

A total of 200 images were used to test the accuracy of the ANN in detection of *Plasmodium* parasites. 100 images had infected erythrocytes while the other 100 images were not infected. The results obtained were tabulated in Table 5.1.

Table 5.1and gives the *Plasmodium* parasite detection accuracy. From the results, the system's detection sensitivity was 92% while its specificity was 97%. This means that the classifier could correctly detect 95 infected erythrocytes out of a total of 100 infected ones. On the other hand the classifier could correctly identify 97 non-infected erythrocytes out of a total of 100 non-infected ones. Out of the total 200 erythrocytes images used, only 11 were falsely classified. This therefore indicates that artificial neural network trained with RGB colour features can be an effective tool for detection of *Plasmodium* parasites. The performance of algorithm developed in this work out performed that of Ross *at al.,* [30] that recorded 85% parasite detection sensitivity. In that work, a total of 37 features were used to train ANN classifier to detect *Plasmodium* parasite. There were a total of 305 samples used to train the network. These were colour features, geometric features and shape features. The current study therefore shows that the performance of ANN classifier can be improved by reducing the dimensionality of the feature vector used as the training set. Specifically, from the results, it can be observed that RGB colour features are sufficient to distinguish *Plasmodium* parasites.

**Table 5.1: *Plasmodium* parasite detection sensitivity**

| | **Subjects with disease** | **Subject without disease** |
|---|---|---|
| **Positive** | 92 | 97 |
| **Negative** | 8 | 3 |

To evaluate the efficiency of the classifier in detection of *Plasmodium*, ROC was computed using the network's outputs and the Targets. A ROC curve was then plotted using values of true positive ratios and false positive ratios obtained from ROC. Figure 5.1 shows the plot. It can be seen that the area under the curve is 1 implying excellent performance of the classifier.

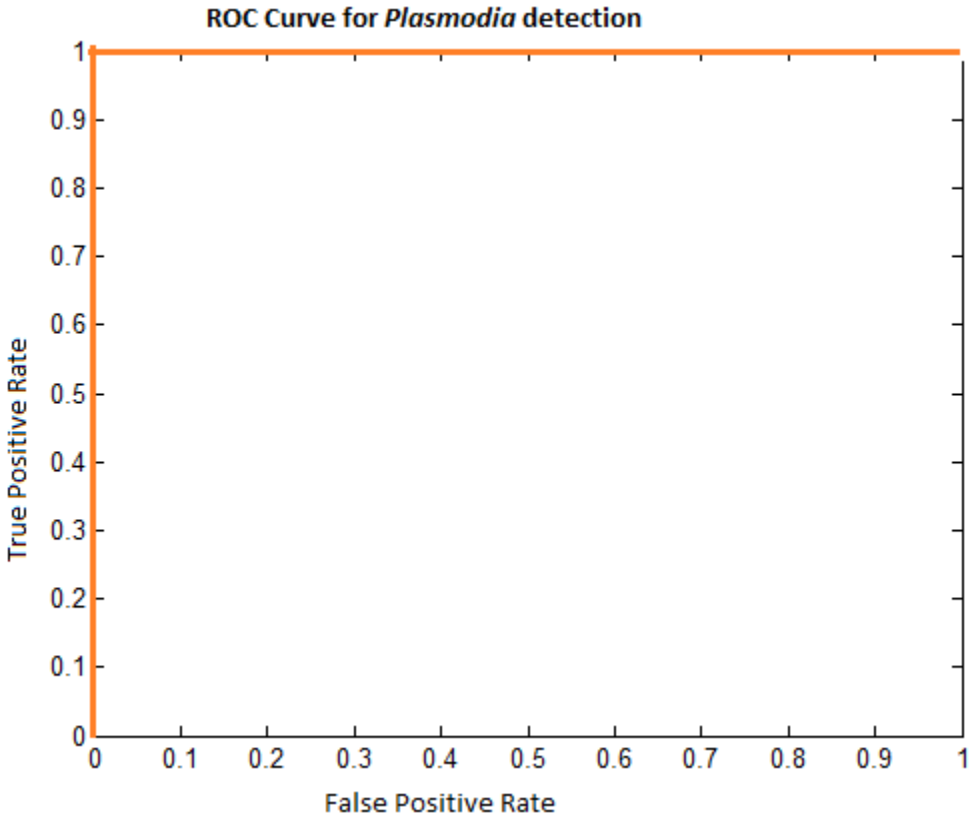


**Figure 4.1: ROC curve for *Plasmodium* detection classifier**

## 5.2 Stages Classification

*Plasmodium* parasite stages identification was performed by a multilayer artificial neural network trained with colour, morphological and texture features of the *Plasmodium* parasites sub-images. The network was trained to recognize four *Plasmodium* life stages; early trophozoite (ring stage), mature trophozoite, gametocyte and schizoint stage. Out of the 205 infected thin blood smear images, 131 were *Plasmodium* parasites at ring stage, 42 erythrocytes had mature trophozoites, 14

had gametocytes and 18 had schizoints. One hundred non-infected erythrocyte images were also used. To evaluate the system's ability to determine stages of *Plasmodium* parasites, both the systems sensitivity and specificity was used. The results of the system are tabulated in Table 5.2.

Table 5.2 gives the stages classification accuracy for the malaria diagnosis system in terms of stages classification sensitivity and specificity. From these results, it is clear that the system could identify ring stage, mature trophozoite and gametocyte stage with fairly high sensitivities i.e. 95%, 90%, and 100%. For schizonts the sensitivity decreased to 72%. The reduced sensitivity associated with schizonts is attributed to few data points used to train the classifier. On the other hand, the high classification accuracy recorded for gametocytes is attributed to the stage's distinct banana shape. The classifier also recorded high specificities as Table 5.2 depicts. This means that the system had very low rates of false positive results. Out of the 305 images used to test the system's ability to identify stages, 190 images were correctly classified. This represents an overall stages classification sensitivity of 92%. The overall specificity of the system was found to be 87%.

The stages classifier was trained with colour, morphological and texture features. As already seen in section 4.2, unlike detection of *Plasmodium* parasites, stages recognition is not adequately determined using colour features. In Di Rubertoand co-workers [33], two techniques were proposed for stages identification. One was the use of colour similarity of the area surrounding the nuclei of the parasite and another was use of morphological skeleton the techniques recorded sensities of 50% and 60% in detection and trophozoite determinationrespectively which are significantly lower that what was found in the current work. It can therefore be concluded that colour features score less than a combination of colour, morphological and texture features in determination of *Plasmodium* parasites stages.

**Table 5.2: Stages classification accuracy for the malaria diagnosis system**

| | Ring stage | Mature trophozoites | Gametocytes | Schizoints |
|---|---|---|---|---|
| **Number of infected images correctly classified (TP)** | 125 | 38 | 14 | 13 |
| **Number of infected images wrongly classified (FN)** | 6 | 4 | 0 | 5 |
| **Number of non –infected images correctly classified (TN)** | 97 | 95 | 100 | 95 |
| **Number of non-infected images wrongly classified (FP)** | 3 | 5 | 0 | 5 |
| **Sensitivity (%)** | 95 | 90 | 100 | 72 |
| **Specificity (%)** | 97 | 95 | 100 | 95 |

To evaluate the performance of the network in *Plasmodium* stages identification, ROC metrics were computed (true positive ratios and false positive ratios) using the network's outputs and the targets used in the training session. Figure 5.2 gives the ROC plot. From this plot the AOC is above 0.8 implying the network performance was impressive.

## 5.3 Species Classification

*Plasmodium* parasite species identification was performed by a multilayer artificial neural network trained with colour, morphological and texture features of both infected erythrocyte images and *Plasmodium* parasites sub-images. To evaluate the system's ability of classifying *Plasmodium* parasites into their correct species, the sensitivity of the classifier was evaluated. This metrics indicates the ability of the classifier to correctly identify the species of *Plasmodium* parasite in an infected erythrocyte image.

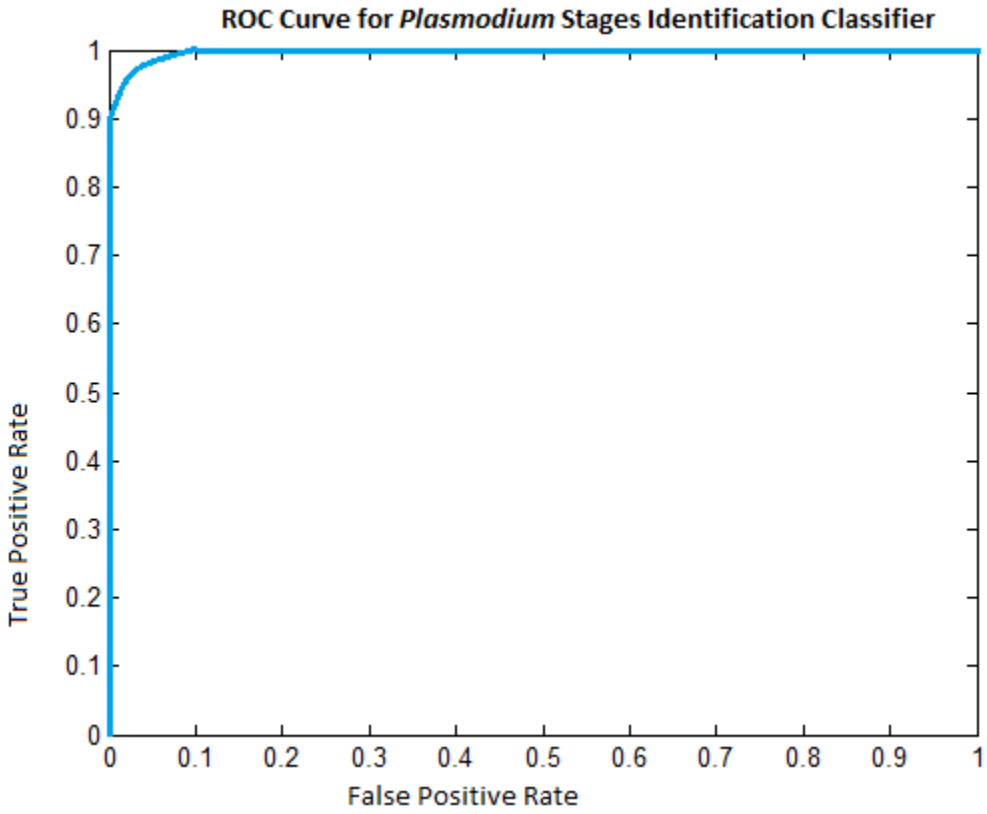


**Figure 5.2: ROC curve for *Plasmodium*parasites stages classifier**

Out of the 205 infected erythrocytes, 80 were infected with *Plasmodium falciparum* parasites, 50 erythrocytes had *Plasmodiumovale*, 50 had *Plasmodiumvivax* and 25 had *Plasmodium malariae* Percentages of the parasites whose species were classified correctly were computed. The results of the diagnosis systemare tabulated in Table 5.3.

**Table 5.3: Species classification accuracy for the system**

| | ***Plasmodium falciparum*** | ***Plasmodium Ovale*** | ***Plasmodium vivax*** | ***Plasmodium malariae*** |
|---|---|---|---|---|
| **Number of images classified correctly** | 76 | 47 | 45 | 21 |
| **Sensitivity (%)** | 95 | 93 | 90 | 83 |

The effect of sample size on performance of the ANN in classification of *Plasmodium* species was also tested. Here, 100 feature vectors were formed using the algorithm described in diagnosis system design methodology. These features were extracted from images infected by the four species of *Plasmodium* parasites. 25 feature vectors were extracted from each of the four groups. These features were then used to train a neural network to classify species. The network was then tested using another set of 100 images comprising of 25 images from each species. The results obtained are given in Table 5.4.

**Table 5.4: Species classification accuracy for ANN trained with 25 feature vectors for each species**

| | ***Plasmodium falciparum*** | ***Plasmodium Ovale*** | ***Plasmodium vivax*** | ***Plasmodium malariae*** |
|---|---|---|---|---|
| **Number of images classified correctly** | 16 | 21 | 16 | 20 |
| **Sensitivity (%)** | 64 | 84 | 64 | 80 |

Tables 5.3 and 5.4 shows the species classification sensitivities for classifiers trained with different numbers of features. In Table 5.3 a total of 205 feature vectors were used while in Table 5.4 a total number of 100 feature vectors were used in training the network.

From the results presented in Table 5.3, the system managed to identify all the species of *Plasmodium* parasites that infect humans with reasonably high degrees of accuracies i.e. 95%, 93%, 90%, and 83% for *Plasmodium falciparum*, *Plasmodiumovale*, *Plasmodiumvivax* and *Plasmodium malariae*respectively. *Plasmodium* falciparum recorded the highest classification accuracy. This is because the classifier was trained with more examples of the parasite features than any other species. On the other hand, *Plasmodium malariae* recorded the lowest classification accuracy since the classifier was trained with the least number of examples of the parasite features

as there were fewer images available of the parasite. This is confirmed by the fact that when ANN was trained by equal number of features (25 feature vectors) from each species, the classification accuracies of *Plasmodium malariae* remained relatively constant (80% down from 83%) while other species classification accuracy reduced significantly. Table 5.4 gives the results obtained after training the ANN classifier with equal number of feature vectors for all the four species of *Plasmodium* parasites. Figure 5.3 shows the ROC curve for *Plasmodium* parasites species classifier. The AOC is above 0.8 which indicates good performance of the network.

## 5.4 Validation of Parasitemia Estimation

Parasitemia was determined by computing the ratio of infected erythrocytes to the total number of erythrocytes in an image. To determine the ability of the system to estimateparasitemia, the parasitemia obtained by the system for the 205 images used were correlated with those obtained by expert microscopists and a correlation coefficient obtained using the following expression [46];

$$r_{x,y} = \frac{E(xy)-E(x)E(y)}{\sqrt{(E(x^2)-E^2(x))(E(x^2)-E^2(x))}} \quad (5.3)$$

where

$x$ = values of parasitemia obtained by expert microscopists

$y$= values of parasitemia obtained by the system

$E$= the expectation value

$r_{x,y}$ = the correlation coefficient between $x$ and $y$

The graph of Figure 5.1 shows the results of parasitemia for both the system and expert microscopists as percentages plotted against the 205 images. Figure 5.1a shows plots of parasitemia against corresponding samples as determined by an expert microscopist and 5.1b show parasite determined by the malaria diagnosis algorithm.The deviations of the predicted values obtained by microscope were presented as error against sample sizes in Figure 5.2.

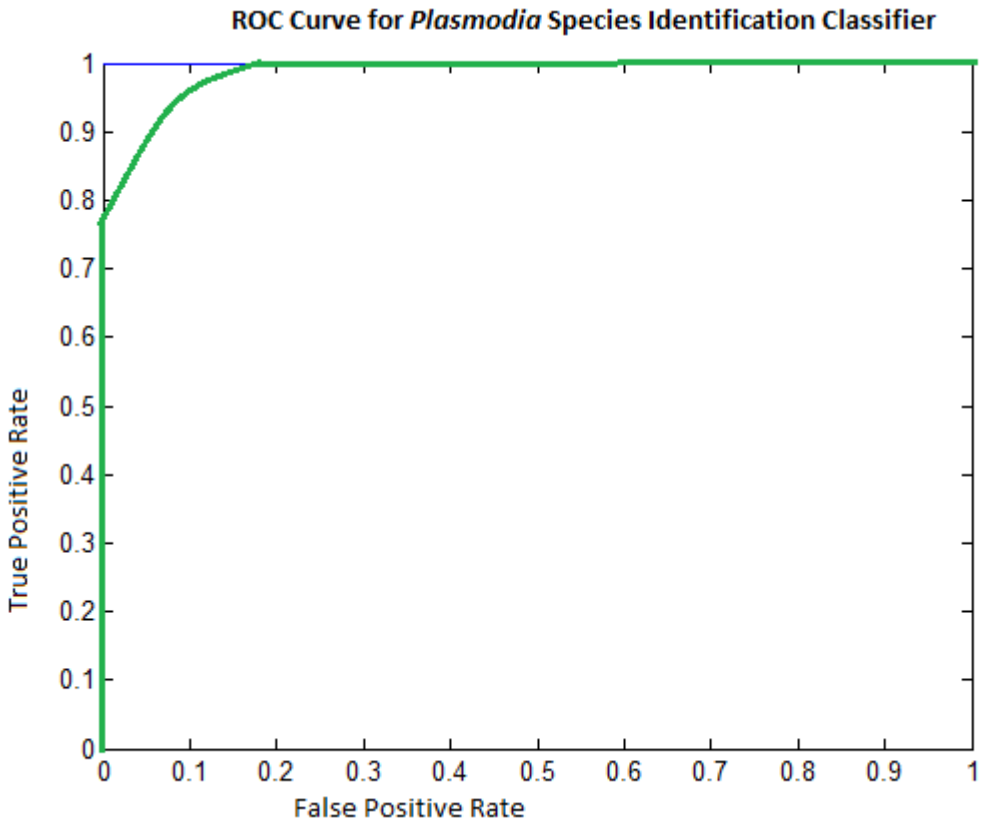


**Figure 5.3: ROC curve for *Plasmodium* parasites species classifier**

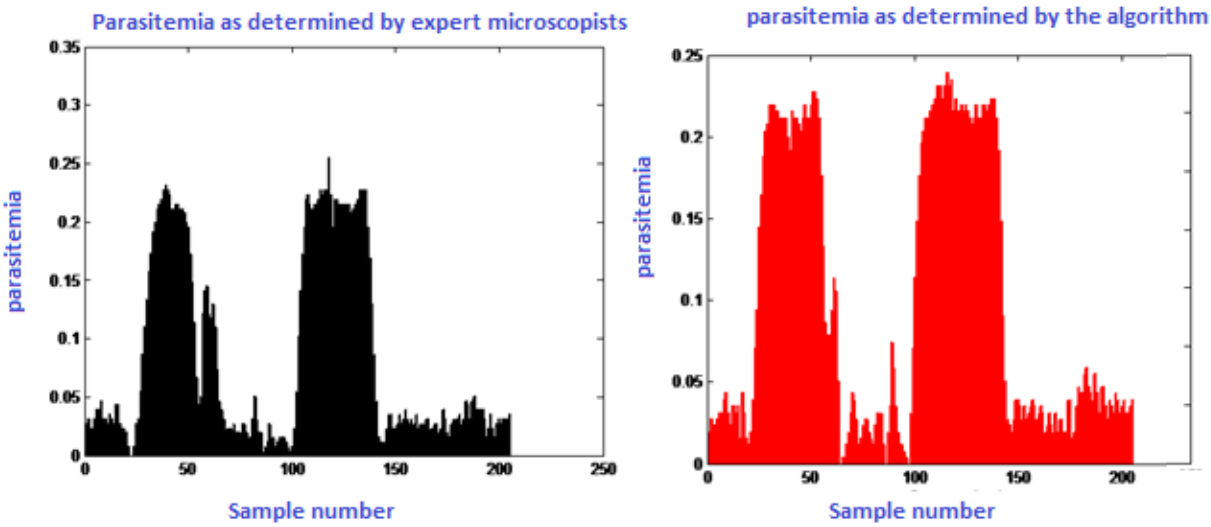


**Figure 5.4: Comparisons of parasitemiaobtained by an expert microscopist (a) and predicted by the algorithm (b)**

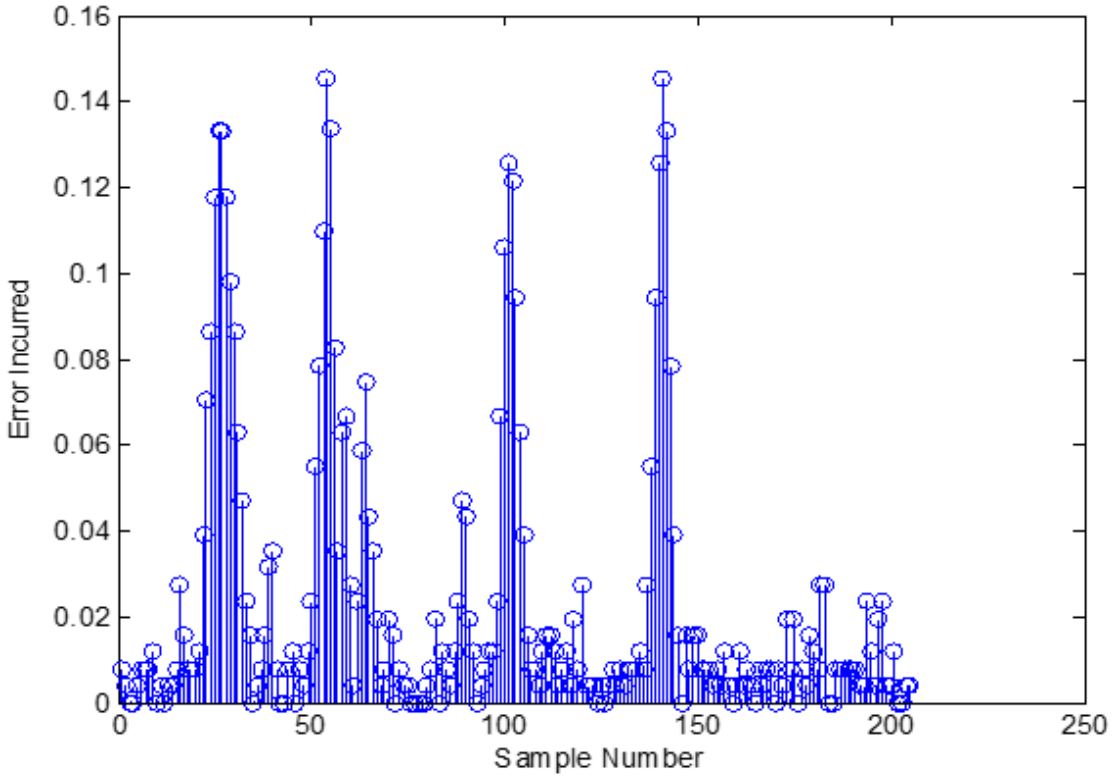


**Figure 5.5: Error incurred by the algorithm for parasitemia estimation**

The correlation coefficient for the data obtained from the two methods was 0.79. This is a strong linear relationship between the developed diagnosis system prediction and the results of expert microscopist given the fact that erythrocytes were highly clustered in the images used. Table 5.5 summarizes the performance of the developed parasitemia estimation technique in comparison to the results obtained by an expert microscopist.

**Table 5.5: Summary of the performance of the proposed parasitemia estimation technique**

| Correlation between the two techniques | Percentage error $\frac{sumoftheerrors}{Totalnumberofsamples} \times 100\%$ | Standard deviation of the proposed technique relative to the results of an expert microscopist |
|---|---|---|
| 0.79 | 21 | 0.062 |

# CHAPTER 6: CONCLUSION AND RECOMMENDATIONS

A system for detecting *Plasmodium* parasites, identifying their life stages and species and estimating parasitemia using images of thin blood smears stained with Giemsa was developed. The outputs of the system were compared to the results of expert microscopists. A total of 205 images were used to train and test the performance of the system. The system recorded 95% accuracy in detecting the presence of *Plasmodium* parasites, 92% in recognizing stages, 92% in recognizing *Plasmodium* species and 79% in estimating parasitemia.

In this work, a novel technique of image segmentation using artificial neural networks trained with pixel values of RGB colour space was developed. The technique was used in segmentation of erythrocytes and *Plasmodium* parasite regions. The results of *Plasmodium* parasites detection showed that ANN classifier trained only with RGB colour features performed better than when the same classifier is trained with both RGB and HSI feature or a combination of RGB, HSI and morphological features. Stages and species recognition algorithm performed better when the ANN classifier was trained using colour, morphological and textural features than using colour features only. It was therefore concluded that detection of *Plasmodium* parasites can be adequately performed by a neural network classifier trained with RGB colour features of the parasite images. On the other hand, stages and species recognition require colour, morphological and textural features to be adequately classified using ANN classifiers. Parasitemia estimation was performed by determining the ratio of infected erythrocytes to the total number of erythrocytes in an image of a thin blood smear sample. To evaluate the number of erythrocytes in a cluster, template matching technique was used. Here, a free standing erythrocyte was searched for in an image and was used a template. This template was run through clusters of erythrocytes and the number of best matches was determined. This was considered to be the number of erythrocyte in the clusters.

Another notable contribution made in this study was the development of a technique for determining the threshold value for segmenting *Plasmodium* parasites from the rest of the blood smear images. The algorithm is a modification of Zack's algorithm for determining global minimum in an image histogram.

A major limitation of this work is the assumption that there would be at least one isolated erythrocyte in a blood sample image to be used as a template. In case no single free standing erythrocyte is encountered, the algorithm's error margin in parasitemia estimation increases. Possibility of incorporating ANN classifiers in estimation of the erythrocyte count may yield better and more reliable results than template match technique. It is also possible to improve on the classification accuracies of detection and differentiation of *Plasmodium* parasite stages and species by using more sample images to extract features from than the present 205 images used in the study. The performance of the technique can further be improved by adopting a standard technique of preparing blood samples and acquiring of sample images.

This work has established a procedure of detecting and classifying *Plasmodium* parasites into their species and stages from images of stained thin blood smears. Further work should focus on ways of improving the process of image acquisition. Optical microscopes are relatively expensive, bulky and require human operators to bring their images into sharp focus. Besides, parasites details are hardly visible without staining of the blood smears, a process which is also time consuming. To reduce these limitations, better image acquisition methods should be explored.

# REFERENCES


1. World Health Organization, (2010), "World Malaria Report 2010", World Health Organization Geneva. Available http://www.who.int/malaria.

2. Snow, R. W., Guerra, C. A., Noor, A. M., Myint, H. Y., and Hay, S. I. (2005). The global distribution of clinical episodes of *Plasmodium* falciparum malaria. *Nature, 434*(7030), *214-217*.

3. World Health Organization, (2011), "World Malaria Report 2011", World Health Organization Geneva. Available http://www.who.int/malaria

4. Warhurst, D.C., and Williams, J.E., (1996), "Laboratory diagnosis of malaria:"*ACO broadsheet no.148, Journal of Clinical Pathology 49,533-538.*

5. Balisle, J.M., Costantino, S., Leimanis, M.L., Bellemare, M.J., Bohle, D.S., Georges, E., and Wiseman, P.W. (2007), "Sensitive detection of malaria infection by third harmonic generation imaging". *Biophysical Journal94(4), L26-L28.*

6. Beadle, C., Long, G. W., McElroy, P. D., Hoffman, S. L., Long, G. W., Weiss, W. R., andOloo, A. J. (1994). Diagnosis of malaria by detection of Plasmodium falciparum HRP-2 antigen with a rapid dipstick antigen-capture assay. *The Lancet, 343*(8897*), 564-568.*

7. Report of joint WHO/USAID (2005):New perspectives of malaria diagnostics, *Informal Consultations, 25-27 October 3 1999.*

8. W.H.O.,(2004),."The role of laboratory diagnosis to support malaria disease management: Focus on the use of rapid diagnostic tests in the areas of high transmission".

9. Uneke, C. J. (2008), "Concurrent malaria and typhoid fever in the tropics: the diagnosticchallenges and public health implications", *Journal of Vector Borne Diseases, 45,133-142.*

10. Iqbal, J., Sher, A., Hira, P.R., and Al-Owaish, R., (1999), "Comparison of the optimal test with PCR for diagnosis of malaria in immigrants", *Journal of Clinical Microbiology, 37, 3644-3646.*

*11.* Kain, K. C., Harrington, M. A., Tennyson, S., and Keystone, J. S. (1998). Imported malaria: prospective analysis of problems in diagnosis and management. *Clinical Infectious Diseases*, *27*(1), *142-149.*

*12.* Singh, B., Bobogare, A., Cox-Singh, J.,Snounou, G., Abdullah, M. S., and Rahman, H. A. (1999). A genus-and species-specific nested polymerase chain reaction malaria detection assay for epidemiologic studies, *American Journal of Tropical Medicine and Hygiene60, 687-692.*

*13.* Snounou, G., Viriyakosol, S., Jara, W., Thaithong, S., and Brown, K.N., (1993), "Identification of four human malaria parasite species in field samples by polymerase chain reaction and detection of high prevalence of mixed infections",*Molecular and Biochemical Parasitology, 58, 287-292.*

*14.* Perandin, F., Manca, N., Calderaro, A., Piccolo, G., Galati, L., Ricci, L., and Chezzi, C. (2004). Development of a real-time PCR assay for detection of *Plasmodium* falciparum, *Plasmodiumvivax*, and *Plasmodiumovale* for routine clinical diagnosis. *Journal of Clinical Microbiology*, *42*(3), *1214-1219.*

*15.* Tjitra, E., Suprianto, S., Dyer, M., Curie, B.J., and Anstey, N.M, (1999). Field evaluation of the ICT malaria pf/pvimmunochromatographic test for detection of *Plasmodiumfalciparum* and *Plasmodiumvivax* in patients with presumptive clinical diagnosis of malaria in eastern Indonesia,*Journal of Clinical Microbiology, 37, 2412-2417.*

*16.* Palmer, C.J., Lindo, J.F., Klaskala, W.I., Quesada, J.A., Kaminsky, R., Baum, M.K., and Ager, L.A., (1998), "Evaluation of the optimal test for rapid diagnosis of *Plasmodium*vivax and *Plasmodium*falaciparum malaria". *Journal of Clinical Microbiology 36, 203-206.*

*17.* Moody, A., (2002), "Rapid diagnostic tests for malaria parasites", J*ournal of Clinical Microbiology Rev.15, 66-78.*

*18.* Mills, C.D., Burgress, D.C.H., Taylor, H.J., and Kain, K.C., (1999), "Evaluation of a rapid and inexpensive dipstick assay for diagnosis of *Plasmodiumfalciparum* malaria",*Bulletin ofWorld Health Organization, 77, 553-559.*

*19.* Gunderson, J.H., Sogin, M.L., Wollett, G., Hollingdale, M., De la cruz, V.F., Waters, A.P., and McCutchan, T.F., (1987), "Structurally distinct stage specific ribosomes occur in *Plasmodium*",*Science 238, 933-937.*

*20.* Kawamoto, F., Miyake, H., Kaneko, O.,Kimura, M., Dung, Liu, Q., Zhou, M., Duc Dao, L., Kawai, S., Isomura, S., and Wataya, Y., (1996), "Sequence variation in the 18sRNA gene, a target for PCR – based malaria diagnosis in *Plasmodiumovale* from southern Vietnam", *Journal of Clinical Microbiology, 34, 2287-2289.*

*21.* Seesod, N., P. Nopparar, Hedrum, A., Holder, A., Thiathong, S., Uhlen, M., and Lundeburg, J., (1997), "An integrated system using immune-magnetic separation, polymerase chain reaction, and colorimetric detection for diagnosis of *Plasmodiumfalciparum*", *American Journal of Tropical Medicine and Hygiene 56,322-328*.

*22.* Sambrook, J., and Russel, D.W., (2001), Molecular cloning: A laboratory manual, (3rd edition) cold spring harbor, N.Y: Cold spring harbor Laboratory press. ISBN 0.87969-576-5: chapter 8; vitro amplification of DNA by polymerase chain reaction.

*23.* Rubio, J. M., Benito, A., Berzosa, P. J., Roche, J., Puente, S., Subirats, M., andAlvar, J. (1999). Usefulness of seminested multiplex PCR in surveillance of imported malaria in Spain. *Journal of Clinical Microbiology*, *37*(10), 3260-3264.

*24.* Snounou, G., Viryakosol, S., Zhu, X. P., Jarra, W., Pinheiro, L., Rosario,V.E., and Thaithong, S., (1993), "High sensitivity of detection of human malaria parasites by the use of nested polymerase chain reaction", *Molecularand Biochemical Parasitology 61, 315-320.*

*25.* Zhong, K., and Kain, K.C., (1999). "Evaluation of colorimetric PCR- Based assay to diagnosis of *Plasmodium* falciparum malaria in travellers",*Journal of Clinical Microbiology 37, 339-341.*

*26.* Webster, G.T., Tilley, L., Deed, S., McNaughton, D., and Wood, B.R., (2008). "Resonance Raman Spectroscopy can detect structural changes in haemozoin (Malaria pigment) following incubation with chloroquine in infected erythrocytes",*FEBS Letters 582, 1087-1092.*

*27.* Zoueu, J. T., Loum, G. L., Haba, C. T., Brydegaard, M. and Menan, H. (2008),"Optical Microscope Based on Multispectral Imaging Applied to *Plasmodium* Diagnosis", *Journal of Applied Sciences8,*(15) ,*2711-2717*.

*28.* Brydegaard, M., Merdasa, A., Jayaweera, H., Alebring, J., and Svanberg, S., (2011), "Versatile multispectral microscope based on light emiting diodes"*Review of Scientific Instruments, 82, 123106*.

*29.* Ross, N.E., Pritchard, C.J., Rubin, D.M, and Duse, A.G., (2006) "Automated image processing method for the diagnosis and classification of malaria on thin blood smears", *Medical and Biological Engineering and Computing,44, 427-436*.

*30.* Omucheni, D.L., (2012), "Multispectral imaging of human blood media applied to malaria diagnosis", M.Sc thesis, University of Nairobi.

*31.* Tek, F.B., Dempster, A.G., and Kale, I., (2009), "Computer vision for microscopy diagnosis of malaria", *Malaria Journal 8(1), 153.*

*32.* Diaz, G., Gonzalez, F.A., and Eduardo, R., (2009),"A semi- automatic method for quantification and classification of erythrocytes infected with malaria parasites in microscopic images",*Journal of Biomedical Informatics 42, 296-307.*

*33.* Di Ruberto, R.C., Dempster, A., Khan, S., and Jarra, B. (2002) "Analysis of infectedblood cell images using morphological operators", *Image andVision Computing20, 133-146.*

*34.* Anand, A.,Chhaniwal, V.K., Patel, N.R., and Javidi, B., (2012), "Automatic identification of malaria infected RBC with digital holographic microscopy using correlation algorithms", *Journal of Photonics, IEEE, 2012.2210199/1943-0655*

*35.* Gonzalez, R.C., and Woods, R.E., Digital Image Processing, 2nd edition, *Prentice Hall of India, New Delhi – 110001,2008*

*36.* Gonzalez, R.C., Woods, R.E., and Eddins, S.L., Digital Image Processing using MATLAB, 2nd edition, (2009), *Pearson Prentice Hall, Upper Saddle River, NJ07458.*

*37.* Solomon, C., and Breckon, T., Fundamentals of Digital Image processing. A Practical Approach with Examples in Matlab, (2010), *John Wiley and sons, West Sussex, P.O. 198SQ, UK.*

*38.* Otsu,N., (1979), "A threshold selection method from gray level histograms",*IEEE Transactions onSystems, Man and Cybernetics, SMC-9(1), 62-66*.

*39.* Zack, G.W., Rogers, W.E., and Latt, S.A., (1977), "Automatic measurement of sister chromatid exchange frequency", *Journal of Histochemistry and Cytochemistry, 25(7), 741-753.*

*40.* Hagan, M.T., Demuth, H.B., and Beale, M., (1996), Neural Network Design, *PwsPublishing Company, Boston.*

*41.* http://www.kemri.org, 1/10/2011.

*42.* http://www.dpd.cdc.gov/dpdx/HTML/ImageLibrary/Malaria_il.htm, 1/10/2011.

*43.* Bansal, R.K., Goel, A., and Sharma, M.K., (2009). MATLAB and its Applications in Engineering,*Pearson Education South Asia, New Delhi, India.*

*44.* Storey, J., (2010), Basic Malaria Microscopy: Part 1. Learner's Guide, *World Health Organization, Geneva.*

*45.* Hagan, M.T., Demuth, H. B., and Beale, M., (2010), Neural Network Toolbox™ 6, *The Mathworks, Inc. 3 Apple Hill Drive Natick, MA 01760-2098*

*46.* Foley, D.H.,(1972), "Consideration of sample and feature size", *IEEE Transactions on Information Theory, IT-18, 618 – 626*

*47.* Hughes, G.F.,(1968), "On the mean accuracy of statistical pattern recognition", *IEEE Transactions on Information Theory, IT-14, 55 - 63*

*48.* Spiegel, M., and Stephens, L.J.,(1998), Statistics, 3rd edition,*Tata McGraw-Hill publishing company Limited, 7 west Patel Nagar, New Delhi 110 008.*

# APPENDIX: MATLAB CODE

## A.1: Image Preprocessing

Code for reading an image from the source file and doing some basic preprocessing.

```
function [Irgb,Ihsv] = imagePreprocessing()
% IMAGEPREPROCESSING() read an image from the source file and filters somes
%random noise and the converts the image to hsv colour space.


Irgb=imread('C:\Documents and Settings\Administrator\Desktop\project\Plasmodiumfalciparum23.jpg');
%convert image to hsv space
Ihsv=rgb2hsv(Irgb);
%perform median filtering on hsv image
Ihsv(:,:,1)=medfilt2(Ihsv(:,:,1),[5,5]);
Ihsv(:,:,2)=medfilt2(Ihsv(:,:,2),[5,5]);
Ihsv(:,:,3)=medfilt2(Ihsv(:,:,3),[5,5]);
%perform median filtering on rgb image
Irgb(:,:,1)=medfilt2(Irgb(:,:,1),[5,5]);
Irgb(:,:,2)=medfilt2(Irgb(:,:,2),[5,5]);
Irgb(:,:,3)=medfilt2(Irgb(:,:,3),[5,5]);
```

## A.2:Segment Erythrocyte:

Code for segmenting Erythrocytes.

```
function E = segmentErythrocyte(Ic)
%E=SEGMENTERYTHROCYTE(IC) recieves a rgb image Ic and returns a binary
%image of erythrocytes.

%get the green component of the image
Ig1=Ic(:,:,2);
%evaluate the threshold value using otsu method
 T=graythresh(Ig1);
%use the threshold to segment the image
 E=(Ig1<T*255*0.95);

%fill the holes
E=imfill(E,'holes');
%eliminate un-necessary objects
E=bwareaopen(E,300);
close all
```

## A.3: Erythrocyte Cropping:

**Code for cropping individual Erythrocytes from the colour images.**

```
FunctionIcc=crop(I,E)
%CROP(I,E) recieves two parameters, I, the preprocessed colour image and E,
%the binary image of erythrocytes and returns subimages of cropped
%erythrocytes.
%quantify the number of erythrocytes
[label,n]=bwlabel(E);
```

```
%get the coordinates of the erythrocyte bounding rectangles
stats=regionprops(label,'BoundingBox');
%crop the erythrocyte sub-images
for x=1:n
r=stats(x).BoundingBox;
Ic=imcrop(I,r);
Icc(x)=Ic;
end
```

## A.4: FeatureVectors:

**Code for extracting features from erythrocyte to aid detection of *Plasmodium* parasites.**

```
function f = featureVector(I)
%F = FEATUREVECTOR(I) receives erythrocyte subimages,I, and extracts colour
%and texture information of the erythrocytes.

% extract colour features
c=colourDescriptors(I);
%extract texture features
Ig=rgb2gray(I);
[t] = statxture(Ig);
st=max(size(t));
sc=max(size(c));
%combine both features
f(1:sc)=c;
f(sc+1:sc+st)=t;
```

## A.5: Colour Descriptors:

**Code for implementing colourDescriptors function**

```
function c = colourDescriptors(I)
%C = COLOURDESCRIPTOR(I) receives an erythrocyte subimage, I, and computes
%defferent colour descriptors.

%convert image to double class
I=im2double(I);
%compute various colour statistics
fori=1:3
krgb(i)=kurtosis(imhist(I(:,:,i)));
end
hsv=rgb2hsv(I);
fori=1:3
khsv(i)=kurtosis(imhist(hsv(:,:,i)));
end
fori=1:3
srgb(i)=skewness(imhist(I(:,:,i)));
end
fori=1:3
shsv(i)=skewness(imhist(hsv(:,:,i)));
end
mrgb=mean2(I);
mhsv=mean2(hsv);
```

```
c=[krgb(1) krgb(2) krgb(3) khsv(1) khsv(2) khsv(3) srgb(1) srgb(2) srgb(3)...
mrgbmhsv];
```

## A.6: Detection of Infection

**Code for testing whether an erythrocyte is infected or not.**

```
function y = detectInfection(I)
%Y=DETECTINFECTION(I) recieves an erythrocyte sub-image and returns one
%of the two values 1 or 0. if y=1; the
%erythrocte is infected and if y=0 it is not infected

%extract necessary features
f = featureVector(I);

%load the neural network classifier which has been trained to detect
%infection
load net4

%classify the erythrocyte
y=sim(net4,f');
if y>=0.5
   y=1;
else
   y=0;
end
```

## A.7: Segmentation of *Plasmodium* Parasite

**Code for segmenting Erythrocytes.**

```
Functionpp = segmentParasite(Ic)
%PP=SEGMENTPARASITE(IC) returns a binary image of potential Plasmodium
%parasite given a subimage of an infected erythrocyte
Ig=Ic(:,:,2);
%get the histogram of the green component image
h=imhist(Ig);
 T=graythresh(Ig);
hh=h(1:T*255);
%apply zacks algorithm to segment parasites objects
T=zacksAlg(hh,Ig);
pp=Ig<T*0.95;
close all
```

## A.8: ParasiteFeatures

**Code for extracting features from erythrocyte to aid in classification of *Plasmodium* parasites life stages.**

```
Functionpf = parasiteFeatures(IB)
```

```
%PF = PARASITEFEATURES(IB) recieves a binary image of a potetial parasite
%IB and computes a feature vector of 20 elements.


[label,N]=bwlabel(IB);
stat=regionprops(IB,'Area','Eccentricity','EulerNumber','Extent',...
'Perimeter','ConvexArea','FilledArea','solidity','MajorAxisLength',...
'MinorAxisLength','EquivDiameter');
[junk,j]=max([stat.Area]);
S = momentInv3(label==j);
FormFactor=(4*pi*stat(j).Area)/stat(j).Perimeter^2;
Roundness=(4*stat(j).Area)/(stat(j).MajorAxisLength^2*pi);
AspectRatio=stat(j).MajorAxisLength/stat(j).MinorAxisLength;
Compactness=((4*stat(j).Area)/pi)/stat(j).MajorAxisLength;

%maxArea=stat(j).Area;
meanArea=mean([stat.Area]);
meanEccentricity=sum([stat.Eccentricity])/N;
meanEulerNumber=stat(j).EulerNumber;
meanExtent=sum([stat.Extent])/N;
meanPerimeter=sum([stat.Perimeter])/N;
meanConvexArea=sum([stat.ConvexArea])/N;
meanFilledArea=mean([stat.FilledArea]);
meanSolidity=mean([stat.Solidity]);
meanMajorAxis=mean([stat.MajorAxisLength]);
meanMinorAxis=mean([stat.MinorAxisLength]);
meanDiameter=mean([stat.EquivDiameter]);

pf=[FormFactor,Roundness,AspectRatio,Compactness,meanArea,meanEccentricity...
   meanEulerNumber,meanExtent,meanPerimeter,meanConvexArea,meanFilledArea,...
   meanSolidity,meanMajorAxis,meanMinorAxis,meanDiameter,S(1,1),S(1,2),S(1,3),S(1,4),N];
```

## A.9: *Plasmodium* Parasite Stages Features

**Code for testing the stage of *Plasmodium* parasite detected.**

```
function y = parasiteFeatures(I)
%Y=PARASITEFEATURES(I) recieves a parasite sub-image and returns a value %corresponding to the
parasite life stage
%extract necessary features
f = parasiteFeatures(I);
%load the neural network classifier which has been trained to classify the parasite into its life stage.
load netstages2
%classify the erythrocyte
y=sim(netstages2,f');
%classify as ring stage if;

if y<10
   y=1;
%classify as band/basket form stage if;
else if (y>10 && y<=20)
   y=2;
%classify as gametocyte stage if;
else if (y>20 && y<=30)
```

```
   y=3;

%classify as schizoint stage if;
else if (y>30 && y<=40)
   y=4;
end
end
end
end
```

## A.10: speciesFeatures

**Code for extracting features from erythrocyte to aid in classification of *Plasmodium* parasites species**

```
function f = speciesFeatures(Ic)
%SPECIESFEATURES extract the following features from an infectected
%erythrocytes(Ic): number of rings in an infected erythrocyte(N), shape of the
%rings(S1), position of the ring reletive to the centroid(d), shape of the
%infected erythrocyte(S2), and texture of the infected erythrocyte(t)


%compute the number of rings in an infected erythrocyte
p=segmentParasite(Ic);
p=bwareaopen(p,20);
p=imclose(p,strel('disk',3));
[label,N]=bwlabel(p);
E=segmentErythrocyte(Ic);
E=imfill(E,'holes');

%calculate the shapes of the rings
for k=1:N
pp=label==k;
pp=imfill(pp,'holes');
   S1(k,:)=momentFeatures(pp);


%compute position of the erythrocyte relative to the centroid of the infected
%erythrocterelative
   stats1=regionprops(pp,'Centroid');
   stats2=regionprops(E,'Centroid','MajorAxisLength');
   c1=stats2.Centroid;
   c2=stats1.Centroid;
   x=abs(c1(1,1)-c2(1,1));
   y=abs(c1(1,2)-c2(1,2));
   d=sqrt(x^2+y^2);
dd=stats2.MajorAxisLength/2;
   d(k,:)=d/dd;
end

%compute shape of infected erythrocye
   S2=momentFeatures(E);
```

```
%compute texture of the infected erythrocyte
Ig=rgb2gray(Ic);
  t=statxture(Ig);
%Code for combining the feature of function speciesFeatures(Ic)
          ms1=max(max(S1));
          ms1=max(size(S1));
          ms2=max(size(S2));
          mt=max(size(t));
          sum=ms1+ms2+mt+2;
          f=zeros(1,24);
          f(1,1)=N;
          f(1,2:1+ms1)=S1(1,:);
          f(1,2+ms1)=d(1,1);
          f(1,3+ms1:2+ms1+ms2)=S2(1,:);
          f(1,3+ms1+ms2:2+ms1+ms2+mt)=t(1,:);
```

## A.11:Determination of Species:

**Code for classifying *Plasmodium* parasites into their species.**

```
function y = determineSpecies(Ic)
%Y = DETERMINESPECIES recieves an infected erythrocyte sub-image and return
%a value of y corresponding to their respective species.
f = speciesFeatures(Ic);
load netspecies2
y=sim(netspecies2,f');
%classify as p.falciparum if;
if (y<10)
   y=1;
%classify as p.malariae if;
elseif (y>10 && y<=20)
   y=2;
%classify as p.Ovale if;
elseif (y>20 && y<=30)
   y=3;
%classify as p.Vivax if;
elseif (y>30 && y<=40)
   y=4;
end
end
end
end
```

## A.12: Number of Erythrocyte:

**Code for determining the number of erythrocytes in a image.**

```
function n= numberofErythrocyte(Ed,EEd)
 [I_SSD,I_NCC,Idata]=template_matching(Ed,EEd);
```

```
[xInyInzIn] = localMaximum(I_NCC);
s=max(size(xIn));
p=1;
vv=0;
y=0;x=0;
for e=0:s-1
 v=I_NCC(xIn(e+1),yIn(e+1));
if  v>0.55 &&EEd(xIn(e+1),yIn(e+1))==1
    x(p)=xIn(e+1);
    y(p)=yIn(e+1);
vv(p)=v;
    p=p+1;
end
end
n=max(size(vv));
imshow(EEd)
hold on
 scatter(y,x,'r')
```

## A.13: Perceptron Rule

**code for implementing the perceptron rule**

```
function [w,b] = perceptron_rule(p,t)
% PERCEPTRON_RULE computes the weight, w, and bias, b, of a single neuron
sp=max(size(p));
w=0;
b=0;
e=1;
while e~=0
fori=1:sp;
        a=hardlim(w*p(1,i)+b);
        e=t(1,i)-a;
        w=w+e*p(1,i);
        b=b+e*b;
end
end
```